Reprinted from

Proceedings of the International School of
Physics «Enrico Fermi» Course CXLIV
M. Allegrini, N. García and O. Marti (Eds.)

V. SANDOGHDAR

Trends and developments in scanning near-field optical microscopy

IOS Press Amsterdam, 2001

Proceedings of the International School of Physics "Enrico Fermi"
Course CXLIV, M. Allegrini, N. García and O. Marti (Eds.)
IOS Press, Amsterdam 2001

Trends and developments in scanning near-field optical microscopy

V. SANDOGHDAR

Department of Physics, University of Konstanz - Konstanz, Germany

1. – Introduction

The early optical microscope opened the door to taking a deeper look into our surroundings and facilitated several important discoveries in science such as that of biological micro-organisms and of the Brownian motion. By the late nineteenth century the theoretical foundations of classical electromagnetism as well as the shortcomings of optical microscopy were understood and formulated. It was realized that the wave nature of light at wavelength λ dictates a limit of the order of $\lambda/2$ on its localization, putting an end to hopes of achieving arbitrarily high resolution in optical microscopy. After the birth of quantum mechanics and the concept of matter waves it was demonstrated that the large momenta and small de Broglie wavelengths of massive particles such as ions and electrons could be exploited for ultra-high resolution microscopy. As a result Scanning Electron Microscopy (SEM) and Transmission Electron Microscopy (TEM) were born and have since become standard techniques, offering spatial resolution under one nanometer.

With the rapid boom in the micro-electronics industry and nanotechnology highly confined fields (*e.g.*, of photons or electrons) have attracted a somewhat renewed attention both in characterization and fabrication of ever smaller features. Nanostructures much smaller than 100 nm are in fact also very interesting from the point of view of fundamental sciences. Such structures consisting of only a few hundred atoms in each direction are often heavily influenced by the quantum effects that result from a finite size and represent a bridge between the quantum-mechanical world of atoms and classical realm of bulk matter.

Although in a "gedanken" experiment we talk about individual atoms or nanostructures such as quantum dots, experimental studies are typically performed on ensembles. The reason for this is first, that locating and isolating individual tiny particles is a nontrivial task. Second, the signal from such one particle is many orders of magnitude weaker than from an ensemble and is often comparable with various sources of noise in the measurement. Nevertheless, in the past two decades scientists have made a tremendous progress in approaching the dream of studying and manipulating individual nanoscopic particles. In particular Scanning Probe Microscopy (SPM) techniques have contributed a great deal to the feasibility of single particle studies. Individual atoms and molecules have been detected and manipulated using Scanning Tunneling Microscopy (STM) [1] and Atomic Force Microscopy (AFM) [2]. Such local methods offer many advantages. Aside from the possibility of eliminating inhomogeneous distributions, the short-range interaction between a sharp probe and the sample can discriminate against the global background signal that could easily become much larger than that of the particle of interest. By the same token, one can locally manipulate or influence the properties of the system. Also, a topographical signal that follows provides valuable insight into the geometry of the problem at hand.

In this course we will focus our attention on Scanning Near-field *Optical* Microscopy (SNOM). Optical information has a unique place in our everyday lives. One could argue that without our eyesight and the ability to see things our perception of the world would have been fundamentally different. We distinguish and differentiate between objects via a range of optically detected measures, such as form, distance, brightness, color, etc. For a physicist colors are of particular importance because they convey very rich information about the absorption and emission properties of atoms and molecules and thereby their internal electronic and vibronic structures. Indeed the fact that the energy level spacings of many substances fall in the visible spectrum and hence are accessible to optical spectroscopy was quite decisive for the early developments of quantum mechanics. Optical methods have been very important in many other areas as well. Having a relatively low energy, an optical photon provides a nondestructive tool for examining various biological processes. Despite its limited resolution, over the years conventional optical microscopy has maintained its status as the most important tool in a biology laboratory because of its versatility, ease of operation under ambient conditions and its compatibility with *in vivo* studies. Having the highest propagation speed, a photon is a prime candidate for information processing and communication. Having well-defined polarization (internal) states, photons tell us about conformational changes in molecular dynamics and can be coded for use in schemes of quantum cryptography. With the recent progress in short laser pulses light beams can also reach astronomically high energy densities, surpassing the Coulomb interaction energy in an atom. Optical sciences and technologies are in fact more than ever in a boom. Some go as far as claiming that photons will replace electrons as the most important particles in science and society of the twenty-first century.

After nearly a century of conviction that optical microscopy cannot contribute to understanding the finest details of tiny organisms, the demonstration of SNOM around 1984 opened new doors [3, 4]. This comeback is nicely shown in fig. 1, that presents a

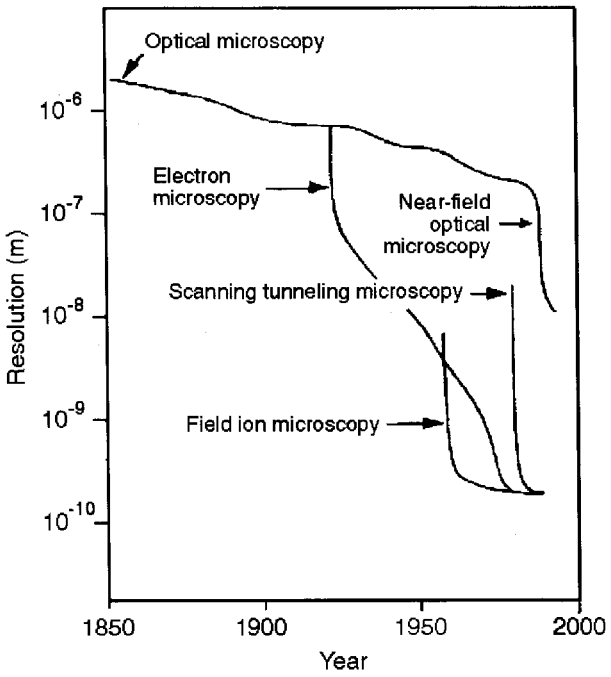

Fig. 1. – The development of different microscopy techniques (taken from [5]).

road map for progress in microscopy over a century and a half. Although the resolution in SNOM remains a few orders of magnitude inferior to that of electron microscopy and related techniques, because of its promise for access to optical properties of matter at the nanometer scale it has created much hope and excitement in the scientific community. The current state of affairs in SNOM resolution is by no means the end of the story; in fact as opposed to its farfield cousin, the resolution in optical near-field microscopy knows no theoretical bounds and limits.

What follows in this course will try to provide a brief theoretical understanding of the limitations in optical microscopy and the foundations of optical near-field microscopy. We will then have a look at the most conventional and historically pioneering form of SNOM, namely the aperture SNOM. Next we will discuss other forms of apertureless optical near-field microscopy that hold promise for reaching molecular resolution. Among these are the use of scattering methods as well as active sources of illumination, such as a single molecule. We close our discussion by sketching some promising aspects of SPM and SNOM techniques for future optical studies.

The compact nature of the current chapter does not allow to review or mention all important contributions and developments in SNOM. This means that we will not be able to present a historically correct account of ideas and their realization. In particular, I have left out the applications of SNOM to semiconductor physics as well as the very

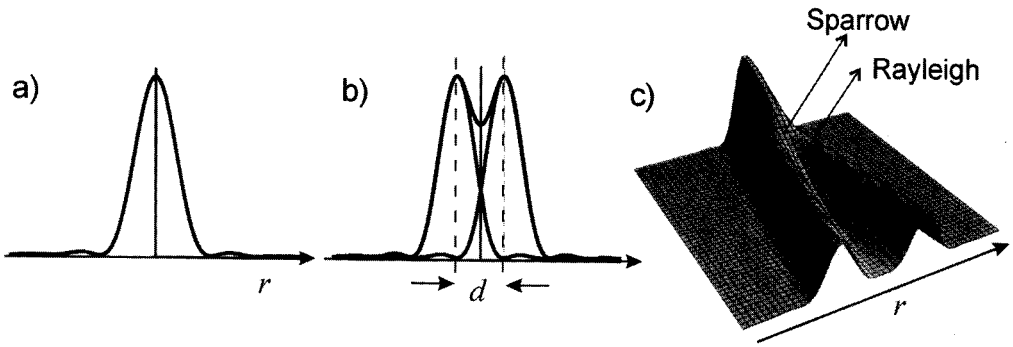

Fig. 2. – a) A cross-section of the radial intensity distribution (Airy function) obtained when a circular aperture is used to image a point. b) Rayleigh criterion: the condition for "just resolving" two point-like objects. c) The signal from two point objects as their separation is varied.

interesting and promising combination of time resolution from short laser pulses with spatial resolution in SNOM. Given a wide range of backgrounds at this summer school, I have decided to take an experimentalist's approach with emphasis on gaining intuition into the field rather than a rigorous and thorough treatment of the subject. So when possible orders of magnitude are discussed in place of formulae and equations. There are several review articles [6-8] and the excellent book by Peasler and Moyer [9] that can be consulted for learning more about this very young and still maturing field.

2. – Resolution in optical microscopy

Nearly every time that we look into a microscope we are curious and excited about seeing the fine details of the object, but we are usually disappointed when even the highest magnification of the best microscope in the laboratory cannot reveal enough information. The fact that every optical device, be it a telescope, camera or microscope has a limited resolution is most commonly explained using an argument by Lord Rayleigh. The so-called Rayleigh criterion was originally proposed for defining the resolving power of a grating spectrometer in which diffraction from slit edges prevents one from obtaining a well-defined spot of light at the exit [10, 11]. In the same manner when imaging a point-like object, diffraction at the edges of a circular objective or mirror also leads to the appearance of ripples around the central spot (see fig. 2a)) in accord to an Airy function. This does not cause any problems if the goal is just to locate the position of a single point-like object. Indeed, several recent works have reported locating single molecules to about 40 nanometers using far-field optics at the visible wavelength [12, 13]; to do this one only requires a good enough signal-to-noise ratio to be able to determine the center of the line shown in fig. 2a). However, if we image two point-like objects of equal intensities and emitting incoherently, the two Airy functions add up, and we obtain a signal as shown in fig. 2b). Rayleigh's criterion for *just resolving* these two points is that

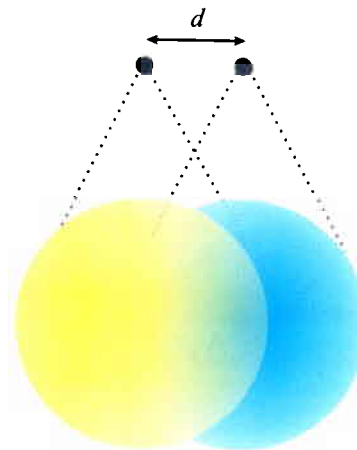

Fig. 3. – A schematic representation of the fluorescence spots from two single molecules with a separation d.

the maximum of one Airy function falls on the first minimum of the second one. This means $d_{\min} \approx 0.6\,\lambda/\text{N.A.}$, where N.A. stands for the numerical aperture of the imaging system [14]. Although this definition is often presented as an absolute criterion, it is quite arbitrary. In fact, other criteria have also been proposed, for example by Sparrow who considered the limit of resolution to occur when the resulting curve has a flat top (see fig. 2c)). In general one could determine the separation d between the two individual curves quite accurately if only the signal-to-noise ratio were high enough and if we knew the exact shapes and intensities of the original lines so that we could fit the signal with the appropriate function. In practice though, this strategy is not viable. Nevertheless, tricks along this line of thought are of current interest in single molecule detection. Consider two molecules fluorescing at two different wavelengths and giving rise to two diffraction-limited spots as shown in fig. 3. Using spectral filters one can separate the two colors and determine the center of each spot quite accurately. In this manner one could determine the separation d between them, *i.e.* resolve them, with an arbitrarily good accuracy. This game can be played every time the two objects carry some identification card such as fluorescence emission, fluorescence lifetime or emission polarization which allow us to separate the two signals [15, 16]. So we see that Rayleigh's definition should not be interpreted as an absolute statement about the limitations of far-field optical microscopy. Nevertheless, it is a very useful criterion for setting a quantitative measure for the performance of an optical system in a *general* situation where one neither knows enough about the sample under study nor does one have enough signal-to-noise ratio to be able to work his way back from a general signal like any cross-section of fig. 2c). In fact, Rayleigh himself explained that "*This rule is convenient on account of its simplicity and it is sufficiently accurate in view of the necessary uncertainty as to what exactly is meant by resolution.*" [14].

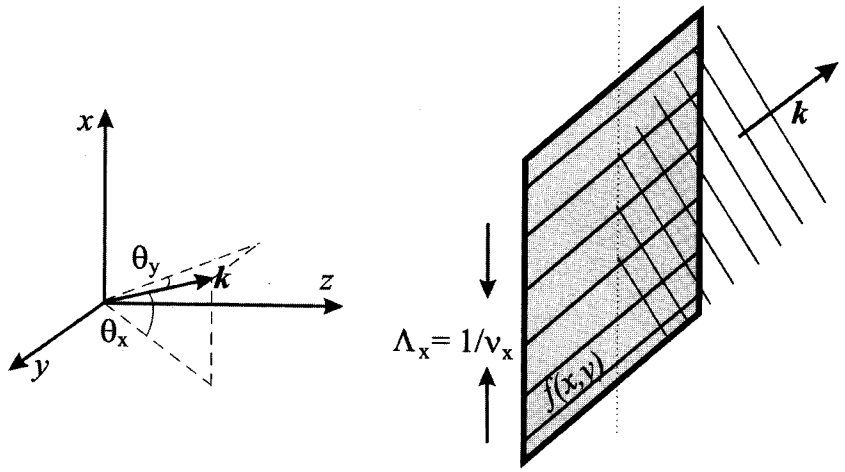

Fig. 4. – The spatial harmonic of a plane wave traveling with wave vector k is shown when $z = 0$ on the object plane. The direction of the propagation is coupled to the spatial frequencies of the spatial harmonics.

In order to establish more solid grounds for understanding the limitations of optical microscopy, let us now follow the Fourier optics approach to imaging as presented in ref. [17]. Assuming the linearity of the optical system at hand (which is quite commonly but not always the case), Fourier optics provides a very powerful tool for analyzing the propagation of light.

Consider a plane wave with amplitude $U(x,y,z) = A\exp[-i(xk_x + yk_y + zk_z)]$ with wave number $k_0 = 2\pi/\lambda = (k_x^2 + k_y^2 + k_z^2)^{1/2}$ and wave vector $\mathbf{k} = (k_x, k_y, k_z)$. The projection of U on the xy-plane, $U(x,y,0)$ can be decomposed into a sum of its spatial harmonics $A\exp[-i2\pi(x\nu_x + y\nu_y)]$, where $\nu_x = k_x/2\pi$ and $\nu_y = k_y/2\pi$ are called its *spatial frequencies*. As depicted in fig. 4, the angles of propagation $\theta_x = \sin^{-1}(k_x/k) = \sin^{-1}(\lambda\nu_x)$ and $\theta_y = \sin^{-1}(k_y/k) = \sin^{-1}(\lambda\nu_y)$ with the yz and xz planes are directly coupled to the spatial frequencies of the wave in the xy-plane.

Given a general monochromatic wave form, we can treat its propagation in free space by considering the fate of each of its spatial harmonics $f(x,y)$ in the xy plane of the object and write $g(x,y) = \int h(x,y)f(x,y)\,\mathrm{d}x\,\mathrm{d}y$ for its projection $g(x,y)$ onto the xy image plane. Here $h(x,y)$ is the *impulse-response* function which tells us what kind of a signal each point on the object plane yields on the image plane; *e.g.*, the Airy function in fig. 2a) is the impulse-response function of a point-like object when imaged with a circular aperture. Equivalently, we can express this propagation in terms of a *transfer function* $H(\nu_x,\nu_y)$ such that $G(\nu_x,\nu_y) = H(\nu_x,\nu_y)F(\nu_x,\nu_y)$, where F, G and H are the Fourier transforms of functions f, g and h, respectively [17]. For propagation over a

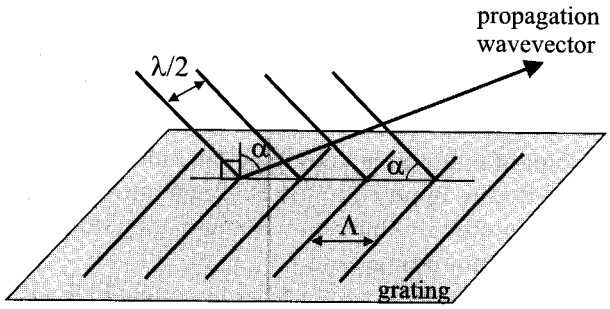

Fig. 5. – The Abbe limit: a diffracted plane wave with wavelength λ can propagate from a grating of period Λ only if $\Lambda > \lambda/2$.

distance d in free space it is easy to show that

$$H(\nu_x, \nu_y) = \exp\left[-ik_z d\right] = \exp\left[-i2\pi d\sqrt{\frac{1}{\lambda^2} - \nu_\rho^2}\right], \tag{1}$$

where $\nu_\rho^2 = \nu_x^2 + \nu_y^2$. Now it becomes clear that if $k_z^2 > 0$, *i.e.* $1/\lambda^2 > \nu_\rho^2$, there exists a propagating wave, whereas if $1/\lambda^2 < \nu_\rho^2$ one obtains *evanescent* or *nonpropagating* waves that decay with an attenuation factor

$$\exp\left[-2\pi d\sqrt{\nu_\rho^2 - \frac{1}{\lambda^2}}\right] = \exp\left[-2\pi d\sqrt{\left(\nu_\rho - \frac{1}{\lambda}\right)\left(\nu_\rho + \frac{1}{\lambda}\right)}\right] \approx \tag{2}$$

$$\approx \exp\left[-2\pi\sqrt{\left(\nu_\rho - \frac{1}{\lambda}\right)\left(\frac{2d^2}{\lambda}\right)}\right]$$

(assuming $\nu_\rho \sim 1/\lambda$). The exponent takes the value $\exp[-1]$ when $2\pi\sqrt{(\nu_\rho - 1/\lambda)(2d^2/\lambda)} \sim 1$. This means that, when $\nu_\rho \gtrsim 1/\lambda$, we require

$$d \ll \frac{\lambda}{2\pi\sqrt{2(\lambda\nu_\rho - 1)}} \tag{3}$$

for the signal to remain of considerable size. In other words, spatial frequencies of the order $\nu_\rho = 100/\lambda$ decay at a length $d \sim \lambda/90$, whereas those with $\nu_\rho = 1000/\lambda$ disappear after $d \sim \lambda/280$.

Recalling that in this treatment we have been dealing with amplitudes and not intensities, we conclude that, in order for a wave to propagate, the spatial frequency of the intensity function (or of the object's optical contrast) has to be smaller than $2/\lambda$. This is the essence of the resolution limit in conventional optical microscopy which states that one cannot obtain information about the fine structures of the sample at spacings

less than $\lambda/2$. One can also arrive at this conclusion by directly examining the grating equation and the condition for obtaining the first-order diffraction from a grating of period Λ at an observation angle α (see fig. 5). It follows that for $\Lambda_{\min} < \lambda/2 \sin\alpha$ one can no longer resolve the grating. This, or its equivalent $\Lambda_{\min} < \lambda/2n \sin\alpha'$ for the case of a surrounding medium of index n, is known as the Abbe limit after Ernst Abbe who formulated it [14]. Note that as opposed to the Rayleigh criterion this limit is exact, but on the other hand the quantitative difference between the two is quite small, which is why the two are often used interchangeably.

Before we leave this section let us take a brief historical look at the efforts that led to the Abbe limit. Around 1870 Ernst Abbe was a lecturer at the University of Jena in Germany where Carl Zeiss operated a microscope factory [18]. At that time although very good microscopes could be made, there existed no scientific approach to their designs. The best microscopes were manufactured by craftsmen with a lot of experience, what Carl Zeiss with his background as a mechanic did not have. So he decided to compete with the established French and English microscope makers by taking a scientific approach. He convinced Abbe to develop a physical theory that he hoped would give him an edge in the microscope business. Abbe started attacking the issue like a physicist, first simplifying the system. The good microscopes of the time all used thick lenses, but Abbe started with thin lenses thinking that the optics would be easier to understand. After many failed experiments that cost Zeiss quite a bit of money he finally located the main issue, the numerical aperture. He realized that the opening angle of the microscope objective, even when not filled with illumination, plays a central role in the sharpness and brightness of the images of wavelength-sized objects. This led him to the conclusion that even the part of the objective that is not illuminated (the "dark space") contained information about the small structures, thus the need for a very high numerical aperture.

Now that we understand where the information about the tiny structures of the object, or rather about its higher spatial frequency components, is hidden, we can come up with some clever tricks to access it. Scanning Near-field Optical Microscopy (SNOM) is the science of this hide-and-seek game. The way it is played is really similar to that of the children's game: A very fine and local probe goes around (is scanned) and finds those in hiding (here the evanescent waves) and drags them out (via scattering).

3. – Basics of SNOM

As we have just seen, the essence of SNOM can be described by acquiring information on the high spatial frequency components of a sample via access to the nonpropagating evanescent waves. However, a thorough and quantitative treatment of the imaging process in SNOM remains a challenging task. Without going into details, let us point out some of the difficulties. As is well known, in the field of diffractive optics solving Maxwell's equations with rough surfaces as boundary conditions is a very demanding job. In particular when the depth of the roughness becomes larger than the typical periodicity multiple scattering becomes important and many analytical or semi-analytical approaches cease to be valid. A complete vectorial calculation of the field distribution

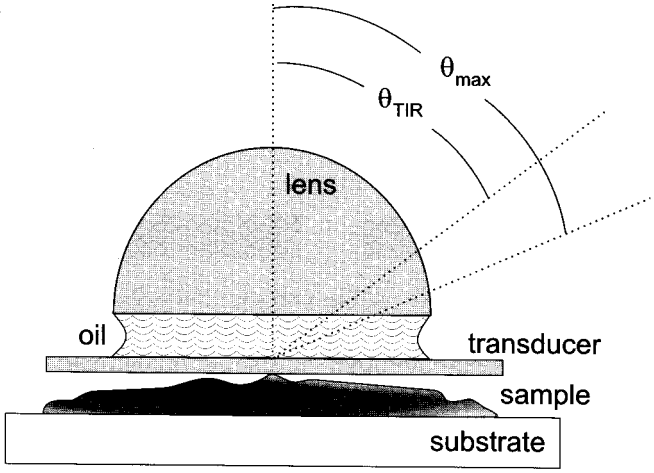

Fig. 6. – The arrangement of an optical tunneling microscope. A microscope objective is modified for imaging the sample in contact. Taken from [9].

on an arbitrary object requires numerical calculations that are much too heavy for a Pentium cluster. This is of course not to say that important steps have not been taken, and as we will see quite a bit is understood. But a rigorous and quantitative description of the near fields is still not routine. We will not discuss any of the numerical methods and refer the interested reader to reviews by Greffet and Carminati [8] and by Girard and Dereux [19].

Here we present an intuitive discussion of optical near-field microscopy. As indicated earlier, the higher the spatial frequencies the faster the signal associated with them decays. In other words, in order to learn about the fine details of the sample we have to get closer and closer to the object surface. You might suggest extracting all the evanescent waves by bringing a prism to an arbitrary small distance from the sample and using a scheme such as frustrated Total Internal Reflection (TIR). This kind of microscope (optical tunneling microscope) actually exists [20,21] and in a certain sense also belongs to the family of near-field optical microscopes. Figure 6 shows the essence of its operation. One obtains very sharp images by bringing an objective nearly in touch with the sample and collecting the high spatial frequency signals at angles $\theta_{\mathrm{TIR}} < \theta < \theta_{\mathrm{max}}$. The details of the illumination and collection techniques and difficulties are more involved and can be found in the parent literature. A brief account of its historical past is given in the book by Peasler and Moyer [9]. Note that this device is in principle not a scanning microscope. A scanning version of it was proposed using a so-called solid immersion lens [22]. As seen in fig. 6, this type of microscope has one important handicap in that its macroscopic size prevents it from exploring the fine topographic features of the sample. For this reason one cannot access the very high spatial frequency components that are confined extremely close to the sample surface. Nevertheless, this arrangement could be favorable

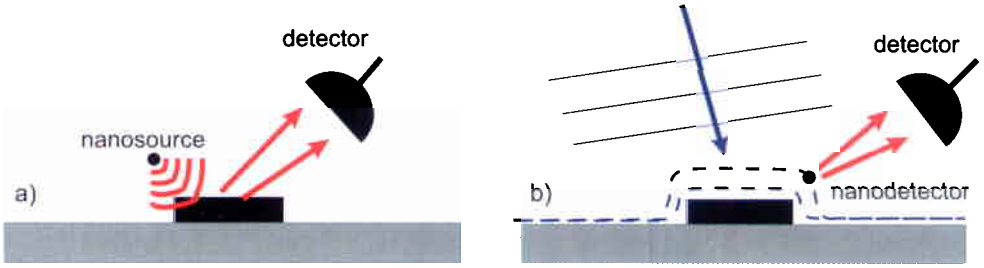

Fig. 7. – Simplified SNOM arrangements. a) The probe is illuminated very locally by evanescent field from a nanosource. b) The sample is illuminated globally and a nanodetector probes the evanescent fields that are created on the surface.

for high-resolution lithography of flat samples [23].

Conventional near-field optical microscopy is performed in the scanning mode using a subwavelength probe that can be brought down to contact with the sample. One can categorize the imaging mechanisms in three main groups: 1) illuminating the object with evanescent waves of a nanoscopic probe (fig. 7a)), 2) illuminating the sample globally in the far field and producing evanescent waves which are then scattered (or *detected*) by the probe (fig. 7b)), and 3) a combination of the two. In all these cases because the information is extracted locally, the lateral size of the probe is a very decisive factor: the smaller the better. A large probe would inevitably scatter the evanescent waves from a large area and therefore lead to washing out the details.

Let us now work through a simple analytic two-dimensional scalar treatment that nicely illustrates the spirit of imaging in SNOM. This approach was first used by Massey [24] and then extended by Vigoureux, Depasse and Girard [25], and is also discussed by Peasler and Moyer [9]. Consider an opaque object to consist of two slits with widths $2L$ and separation $2d$. The field at the aperture can be written as

$$f(x, z=0) = E_0 \,\mathrm{rect}[-d-L, -d+L] + \mathrm{rect}[d-L, d+L] \tag{4}$$

with a Fourier transform

$$F(k_x, z=0) = 4E_0 \cos(k_x d) \frac{\sin(k_x L)}{k_x L}, \tag{5}$$

where $\mathrm{rect}[a,b] = 1$ for $a < x < b$ and is 0 elsewhere. We now can use the transfer function formalism to determine the field at a distance z:

$$f(x,z) = \int_{-\infty}^{+\infty} \mathrm{d}k_x \exp\left[-ik_x x\right] F(k_x, z=0) \exp\left[-iz\sqrt{k_0^2 - k_x^2}\right] \quad \text{for } k_0^2 > k_x^2, \tag{6}$$

and

$$(7)\quad f(x,z) = \int_{-\infty}^{+\infty} \mathrm{d}k_x \exp\left[-ik_x x\right] F\left(k_x, z=0\right) \exp\left[-z\sqrt{k_x^2 - k_0^2}\right] \quad \text{for } k_0^2 < k_x^2.$$

One can take this one step further and convolute (in other words diffract) this field with a probe of width w and integrate the far field. The results of such a calculation are shown for different parameters z and w in fig. 8a) where the *probe* is shown to be also an aperture. The importance of the two parameters, the size of the probe and its separation from the sample, becomes very clear when comparing the signals obtained in various situations. Figure 8b) also shows the Fourier spectrum of the wave field at different z-positions in front of the sample. The high-frequency components disappear at larger distances.

Before we go on to the more experimental part of the course, it is important to emphasize that regardless of the configuration of choice, the responsible mechanism in SNOM is scattering [8]. This is quite different from the most conventional form of optical imaging where reflection, refraction or diffraction are the main players. These concepts are all defined for macroscopic systems and lose their meaning for subwavelength interactions. A nice example for the unintuitive nature of near-field imaging is shown in fig. 9. Here the field intensities in the immediate vicinity of two nanoscopic objects of the same size and geometry but of different indices of refraction are plotted.

3·1. *A note on the uncertainty relation.* – It is well known that the uncertainty relations in quantum mechanics are very closely related to the relationship between Δx and Δk_x in optics where x and k are Fourier transform conjugates of each other. In other words, due to the wave nature of light and of matter waves in both cases $\Delta x \Delta k_x$ fills a nonzero area in the phase space. For light the lower limit is 2π whereas for matter waves this is h. So given this intrinsic link between the two, one might get a feeling that obtaining resolution beyond the diffraction limit, or, in other words, localizing Δx to arbitrarily small regions, could mean violating this rule. However, as Vigoureux and Courjon have pointed out [26], confining Δx simply means a $\Delta k_x > k_0 = 2\pi/\lambda$ and therefore waves that do not propagate. What one does in SNOM is inserting a local probe and freeing these fields. This is not in conflict with any laws of physics.

4. – Aperture SNOM

In this section we take a closer look at the most conventional form of optical near-field microscopy, namely aperture SNOM. The idea here is depicted in fig. 10a). Typically a tapered optical fiber is aluminum coated at an angle so that a very small opening is left at the front where light can exit (see fig. 10b)). This probe is placed in front of the sample at separations of a few nanometers. The light scattered by the sample is then collected in reflection or transmission in the far field and registered using conventional detectors. This means that here instead of detecting the evanescent fields of a sample, one generates evanescent fields at the exit of a subwavelength aperture and scatters them

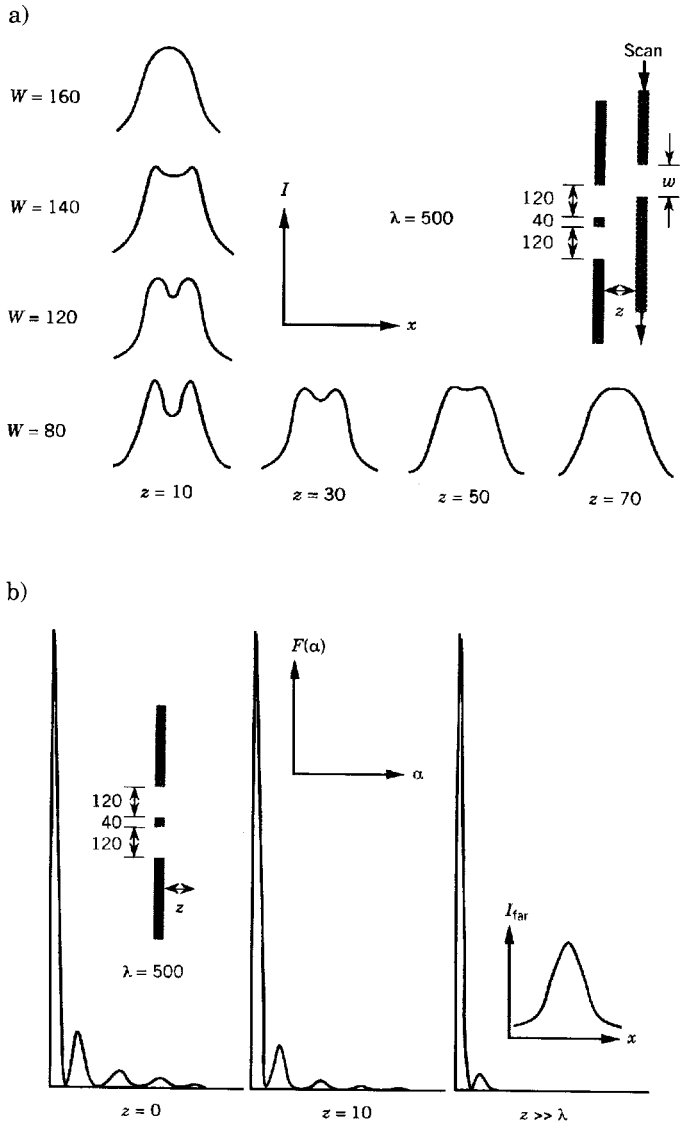

Fig. 8. – A double slit is taken to be an object and is probed by a third slit as a probe. Scalar simplified calculations reveal the essence of imaging mechanism in SNOM. a) The signal obtained for various probe size w and separations z. b) The Fourier spectrum of the double slit at three different distances. Taken from [9].

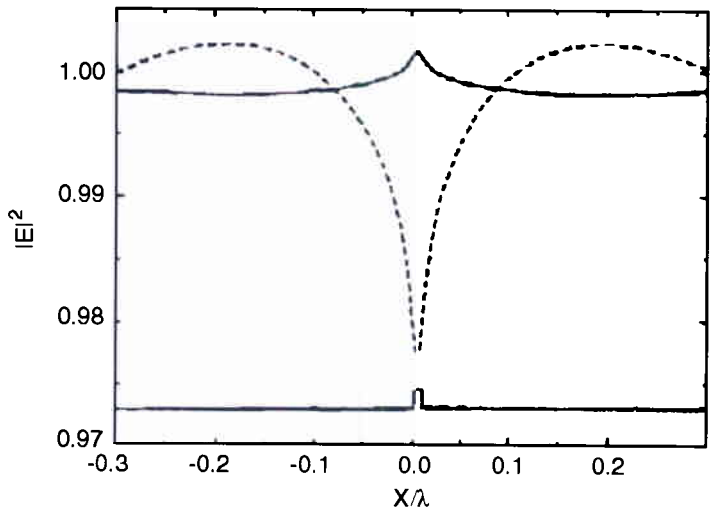

Fig. 9. – Calculated field intensities in front of subwavelength objects made of silver (dashed line) and glass (solid line). Taken from [8].

into the far field by bringing them in touch with the sample. Aside from providing a high resolution, this arrangement has the important advantage that the sample is illuminated very locally, and therefore, there exists essentially no far-field background, an issue that we will confront later in the context of apertureless SNOM.

The imaging mechanism of aperture SNOM is often explained in a simple-minded manner by considering the aperture to act as a pinhole through which one only looks at a subwavelength part of the sample. This argument is naive because it sounds like applying intuition from geometric optics to the subwavelength domain, but one can also formulate it in more rigorous terms. Consider the spatial Fourier components that

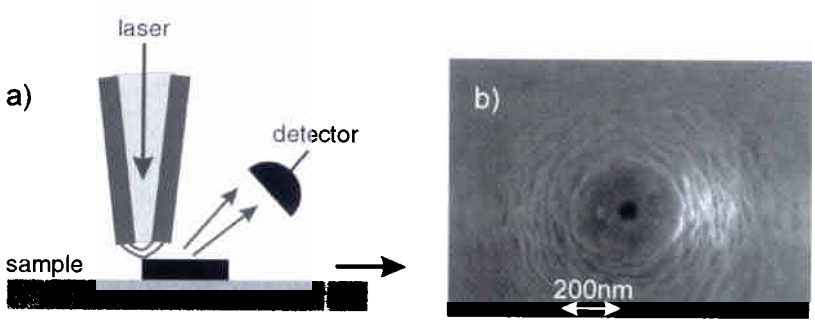

Fig. 10. – a) Schematic representation of SNOM with a coated optical fiber. Evanescent waves at the exit of the aperture are scattered by the sample into the far field. b) A scanning electron microscope image of a *good* tip (source of image unknown).

are produced at the exit of the aperture. Without going into details one can convince oneself that the spatial frequencies available go roughly up to the inverse of the aperture diameter D. So the smaller the aperture the higher the available spatial frequencies that can be scattered by very fine structures of the sample.

Using a tiny aperture was the core of E. A. Synge's first proposal in 1928 for an optical near-field microscope [27]. He suggested metalizing a sharp cone of quartz glass with a radius of about 10 nm and then removing the metal at the very end to create a hole. In fact this is really how one of the first SNOMs was realized by D. Pohl and coworkers at IBM research laboratories in Zürich around 1984 [3]. The approach used by the group of A. Lewis at Cornell University was slightly different and applied metal-coated heat-drawn hollow micropipettes as probes [4]. It is interesting to remember, though, that obtaining high resolution in the near field has been alluded to also by several authors in different contexts as early as the 1950s [9], and that its microwave version was first demonstrated by Ash and Nicholls in early 70s [28]. The reason the *optical* near-field microscope could be only realized in the 1980s was that prior to the invention of STM in 1982 there were no means for stabilizing the probe-sample distance to within a few nanometers. Indeed, both the IBM and the Cornell groups took advantage of electron tunneling current to assure that their fragile probes were not damaged by small sample corrugations. We will not discuss the instrumental and technical aspects of aperture SNOM here since it is amply covered in the literature and addressed in O. Marti's lectures.

4·1. *Field distribution at the aperture exit.* – The field distribution at the exit of a circular subwavelength opening has been calculated by H. Bethe [29] who considered an aperture in an infinitely thin and perfectly conducting plane illuminated at normal incidence. In 1950 Bouwkamp corrected Bethe's calculations [30] in the near-field region. Figure 11 shows some of these results for the square of the field components in different orientations when a linearly polarized light in the x-direction has been incident. These variations have been put into experimental evidence by being mapped with a single dye molecule (see the middle column of fig. 11) [31] or with semiconductor heterostructures [32]. Of particular interest are the existence of substantial z-components in the electric field as well as the rapidly changing character of the intensity profile as a function of distance from the aperture. Note that at a separation of 0.8 times the aperture diameter the field distribution is already very close to Gaussian.

It is also interesting to have a look at the far-field distribution of such an aperture. At first one might not expect any far-field radiation since we have argued that the fields at the aperture are nonpropagating. But in fact a typical SNOM probe emits a few tens of nW, which is easily visible to the naked eyes. The reason for this is that diffraction from a subwavelength hole also entails low spatial frequency components that can propagate. Another way of looking at this is that the incident light induces oscillating electromagnetic moments that correspond to oscillation of charges at the aperture boundary, leading to a near-field as well as a radiating field. K. Karrai and C. Obermüller have examined this by performing angle-resolved measurements of the optical intensity far away from the aperture of a coated optical fiber [33]. Figure 12 shows their results in the plane

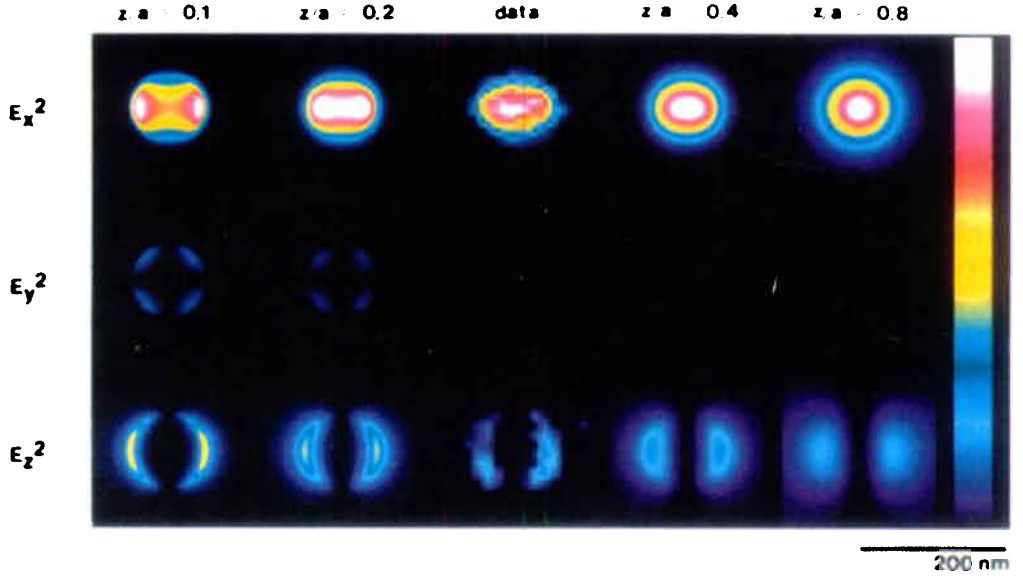

Fig. 11. Field intensity distributions of an aperture as calculated according to the Bethe-Bouwkamp model. Different rows indicate x, y, z polarizations while columns note various separations from the aperture. z is the separation of the aperture from the plane of calculation, and a is the aperture diameter. The middle column labeled data displays experimental results of mapping the field of a coated optical fiber tip by single molecules (taken from [31]).

parallel and perpendicular to the electric field of the incident radiation for apertures of different diameters.

Bethe's model describes the *far*-field pattern by the radiation from a combination of a magnetic- and an electric-dipole moment whereby the magnetic moment should be antiparallel to the magnetic field of the incident radiation and the electric moment parallel to the normal component of the incident electric field, namely zero for normal incidence. In fig. 12 it is evident that as the aperture gets smaller the angular distribution becomes wider. However, one sees that for very small apertures Bethe's result, a flat angular response, is not verified for the detection plane parallel to the incident electric field (fig. 12b)). Also, note that a considerable signal is detected at angles larger than 90°, *i.e.* behind the aperture. In the detection plane normal to the incident polarization one obtains an agreement with the Bethe theory only when considering magnetic and electric dipoles both parallel to the polarization. These measurements show that although the Bethe-Bouwkamp model seems to give a good qualitative agreement with the experiment in the near field [31], they do not agree with the far-field radiation pattern of apertures at the end of a sharp metallized tip. Nevertheless, the authors note that their results could be helpful for rapid and empirical far-field characterization of SNOM aperture probes.

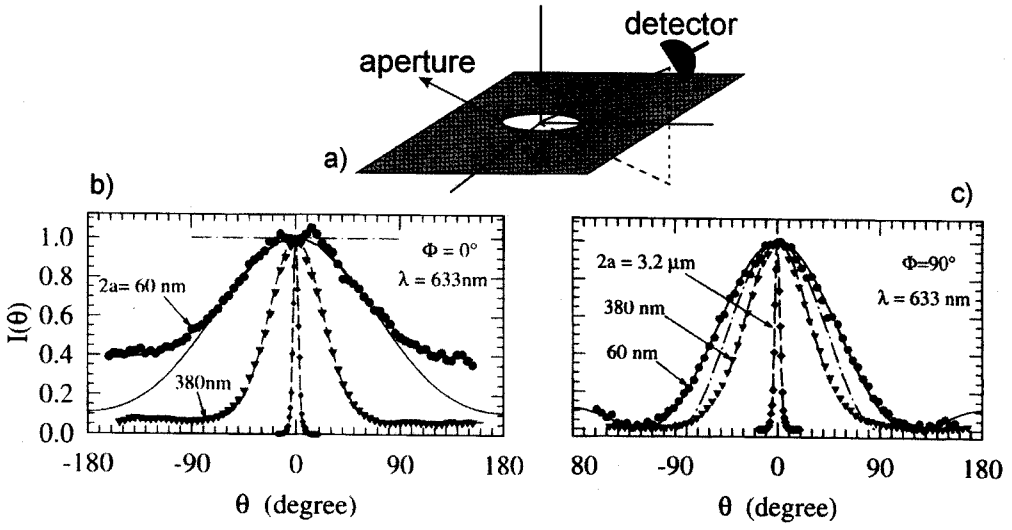

Fig. 12. – a) The arrangement for measuring the far-field intensities exiting various apertures at different angles. The polarization of the incident light is along the $\phi = 0$ axis. b) and c) show the results for detection parallel and perpendicular to the plane of polarization. The dot-dashed lines indicate the predictions of the Bethe model while the solid lines show the best fit to the data (taken from [33]).

4·2. *Light propagation in the probe.* – As we pointed out before, in practice a SNOM probe is like a funnel with a very sharp end. As opposed to conventional funnels, though, in the case of a light funnel we have to be aware of absorption of metal walls as well as the existence of a cut-off for the propagation. Absorption causes heating which could lead to practical difficulties such as damage to the tip or the sample. At the same time the tapered nature of the probe severely limits the amount of light that can arrive at the aperture. Because of this there have been quite a few efforts to optimize the shape of this funnel in order to maximize the output [9]. One of the avenues is using a higher dielectric index and another is to increase the opening angle (reduce the taper) for at least part of the probe in order to postpone the cut-off region or to minimize the length of the taper [34,35]. These ideas are, however, difficult to implement because of fabrication complications as well as problems in quantitative simulation of the light propagation for realistic geometries.

4·3. *Limitations of the aperture* SNOM. – After more than a decade and a half, reproducible and efficient fabrication of aperture probes remains an unsolved technological problem. Several methods have been proposed for producing sharp tips and for their metal coatings. However, none of these techniques have proven to be both reliable and affordable at the same time. Problems vary for each probe conception. In summary one can say that, at an age when nanotechnology has become a topic of everyday conversations, controlling the material properties of a SNOM probe still poses nontrivial

fabrication problems. Some of the problems can be seen in fig. 10b). Although an aperture of about 50 nm is nicely visible, one also notes that the metal coating is far from uniform on the nanometer scale. Small roughness at the tip could influence the optical as well as mechanical aspect of the imaging process.

Aside from the issues of shape and output optimization discussed earlier, one would like to have an aperture as small as possible. Although one might imagine that one day all technological problems could be addressed satisfactorily, it turns out that there is a fundamental lower limit to the size of the aperture. This is caused by the finite skin depth of visible electromagnetic radiation in realistic metals, 6–7 nm for aluminum. This means that even if the aperture were to be geometrically closed, as long as a reasonable amount of light is to exit, one obtains an effective aperture of about 30 nm [36, 37].

5. – Image interpretation

Before we go on to more novel forms of SNOM it is worth discussing some important issues regarding various imaging mechanisms and their interpretations. Any form of microscopy, whether it is the simple-seeming traditional optical microscopy, electron microscopy, STM or AFM, requires a great deal of care in understanding the contrast mechanism at work in order to extract information about the sample and in order to distinguish genuine effects from artifacts. In fact, anyone who has operated an optical microscope knows that the way the sample is illuminated, namely in bright field or dark field in transmission or reflection, can considerably influence the image quality. Things that look bright in one mode could look dark in the other and vice versa. Also changes in the index of refraction could be easily mistaken for changes in the geometrical path length.

Near-field optical microscopy is no exception to this rule. We have already seen in fig. 9 that the mere change of the object material from glass to silver could lead to a completely different image quality. Figure 13 shows an experimental example of polarization dependence in SNOM imaging [38] that was first reported in 1992 by Betzig and coworkers [39]. This rich behavior is dictated by the boundary conditions that have to be satisfied for the field of a given polarization at the edges of a structure with a certain orientation [40, 41]. As a rule of thumb, the simplest image is obtained when the illumination electric field is perpendicular to the substrate because as the probe is scanned across the sample the field component parallel to the substrate experiences a discontinuity while the normal field does not.

5·1. *Artifacts.* – For any specific sample-probe and illumination-detection combinations one has to look for different sets of stray signals and artifacts that might contribute to the image. Here we will only discuss the most common type, the so-called topography-induced artifact. Scientists working with SNOM seem to have been aware of these artifacts from the very beginning [9], but their great potential to do damage has been taken much more seriously in the second half of the 90s, particularly because of the work of D. Pohl and his coworkers [42].

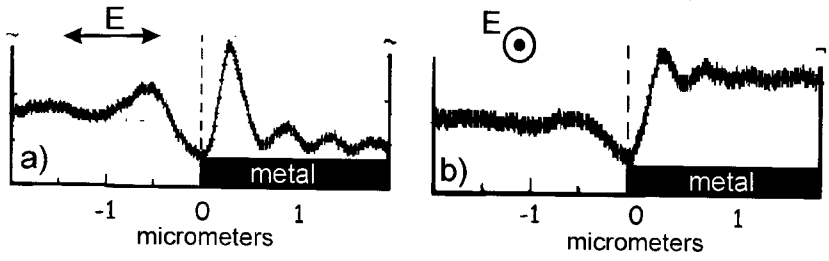

Fig. 13. – The signal recorded from an aperture probe in transmission. The probe is scanned over a metal-glass edge for two different illumination polarizations (modified from [38]).

The optical and topographical signals in SNOM are very closely coupled because of the strong distance dependence of the evanescent waves. It is important, however, to emphasize that this coupling is not what gives rise to topography artifacts. What is understood by topography artifacts in SNOM is an *apparent* contrast that creeps into the image but has its origin in far-field effects. There are two main reasons why topography-induced artifacts are omnipresent in many cases. First, in any realistic arrangement there exist photons that can bounce around many times before landing at the detector. If this multiple reflection or scattering takes place between parts of the probe and of the sample it could lead to interferences. As the probe-sample distance is modulated during the scan, such a signal leads to a contrast on the detector. This apparent contrast has been reported by different groups to reach 1% per 1 nm of tip-sample modulation almost independently of the experimental arrangement [42-44]. This means that imaging a sample that is 10 nm tall could give up to 10% false contrast which could easily dominate or become comparable with the true near-field signal. Figure 14 shows very nicely an example of such stray signals when gold particles are imaged in transmission using a conventional aperture probe [45]. When the tip-sample distance is controlled in the constant gap mode (CGM) z-modulations create a contrast that shows a one-to-one correspondence with the topography image, reproducing very tiny features with the same spatial resolution (the larger gray part in fig. 14b)). In the constant height mode (CHM) these are nearly absent and one only sees a variation in the signal when the aperture comes near the particle. Incidentally, here one can also clearly see the small polarization effects (discussed above in fig. 13) that give rise to bright spots just outside the dark central spot.

Unfortunately the constant height mode does not always result in images that are easy to interpret. Figure 15 shows two examples of samples, a) with lateral contrast in the index of refraction and b) pure topography modulations. While in part a) a CHM scan keeps the interesting near-field signal of the small object on the substrate, in part b) it fails to detect all the evanescent waves that follow the topography modulations of the sample. In general there exists no recipe for removing the topography-induced artifact, and for each experiment one has to consider the details of the imaging mechanism and then perform appropriate checks. As we will see in a concrete example in sect. **6**·2, studying the wavelength dependence of the contrast mechanism can offer useful hints.

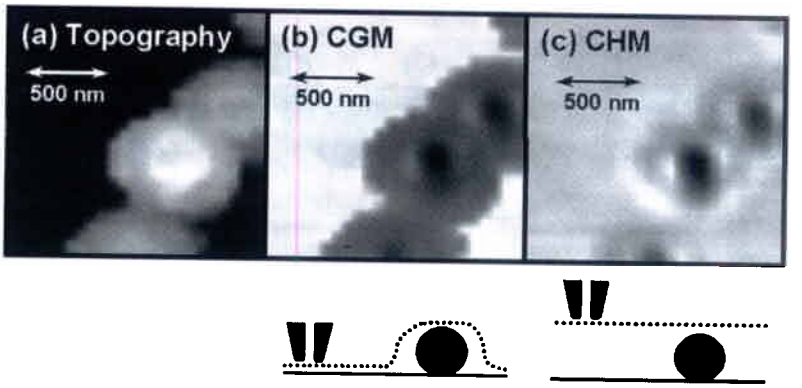

Fig. 14. – a) The topography image of gold nanoparticles. Since the gold particles are smaller than the tip extremity, the spots represent the tip geometry. b) The optical signal collected simultaneously when the tip is scanned over the sample in constant-gap mode. The details of the tip geometry clearly creep into the optical signal. c) The optical signal recorded in the constant height mode. Taken from [45].

Also observation of contrast inversion is often a signature of artifacts [43, 46].

5·2. *A high-contrast topography-free sample.* – Although in a practical microscopy experiment the goal is to learn about an unknown sample or to characterize it in a quantitative manner, for a field as young as SNOM it is very useful to be able to perform controlled experiments on well-characterized test samples. In the light of topography-induced artifacts discussed in the previous section it is particularly desirable to have access to a sample with a high optical contrast and no residual topography. Such a sample results in a marriage between the CHM and CGM scan modes and also has the practical advantage that even a fragile tip can be brought as close to the sample as possible without running the risk of damaging it by the sample roughness.

A good example of a topography-free sample is a collection of single molecules [31] spread on a substrate. However, these systems are not very photostable and their detection with SNOM requires expertise and access to costly equipment. Therefore a few groups have tried ways of producing solid durable test samples. One method has been

Fig. 15. – Schematic representation of the constant height mode (CHM) and constant gap mode (CGM) for tip-sample scanning. While CHM offers advantages for the sample in a) it creates complications for the one in b).

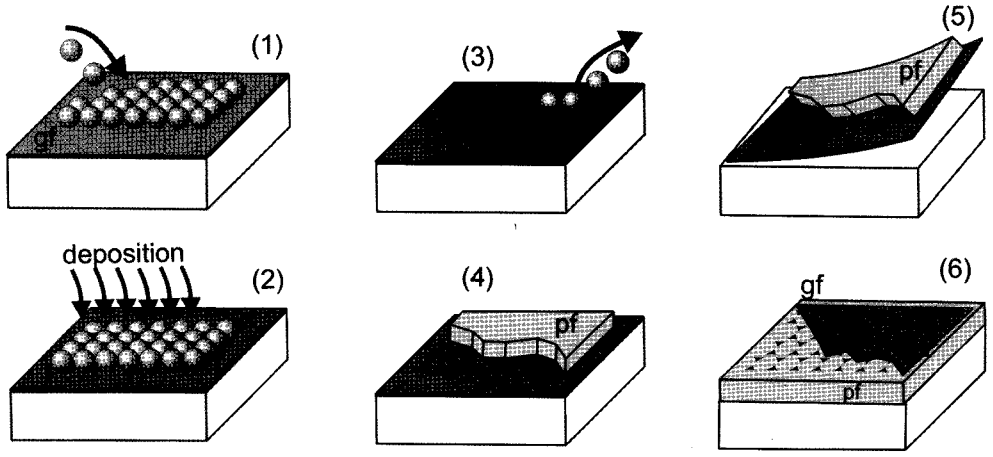

Fig. 16. – The main steps for the fabrication of a topography-free sample with high lateral optical contrast. gf stands for gold film and pf for polymer film.

side cleaving a semiconductor heterostructure [32,47] or a multilayer sandwich of different films. Preparation of such samples requires sophisticated equipment, and the samples usually show low optical contrast. A particularly versatile technique initiated by U. Fischer in the early 80s [48] takes advantage of the self-organization of colloidal particles to produce a mask through which material of different substance, usually metals, can be evaporated onto a substrate (see fig. 16). After removing the colloidal particles one is left with a hexagonal array of islands that could then be covered by a second substance, for example a polymer [48] or another metal [49]. If the underlying substrate is very flat, one could expect the deposited heterostructure to be also as flat. However, it turns out that typically one is left with a small residual topography that is perfectly correlated with the material contrast [49].

In order to get around this problem, one can start with a very thin gold film as shown in fig. 16. This gold film ensures a smooth lift-off of the sample from the underlying substrate, and the resulting interface becomes extremely flat [50]. Figure 17 displays topography and optical images recorded using an aperture probe in shear-force mode. A contrast larger than 20% and an extremely flat topography image without any correlation with the material contrast are all important indicators for a genuine near-field resolution. This sample has the advantage of being inexpensive, easy to make and very flexible since the choice of material and size of the islands can be varied over a large range. Finally, due to its conducting upper layer the tip-sample distance can be controlled via tunneling current for probes that cannot use shear force [49].

6. – Apertureless SNOM with passive probes

6·1. PSTM. – In 1989 two groups independently reported a kind of SNOM that has been referred to as Scanning Tunneling Optical Microscope (STOM) or Photon Scanning

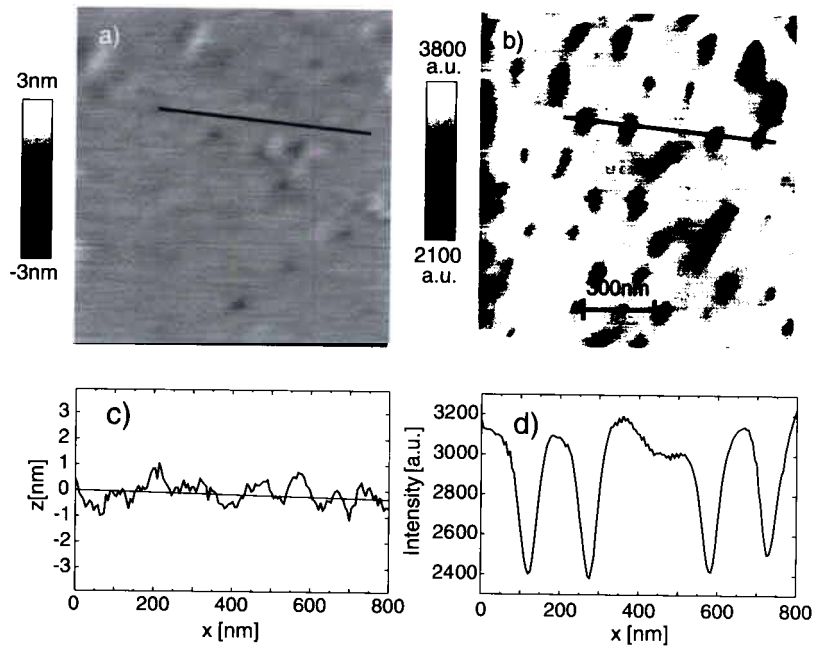

Fig. 17. – a) A topography image of the sample made according to the procedure in fig. 16. b) The SNOM image corresponding to a). The gray scales represents the raw intensities measured in the experiment. c) A cross-section from the cut shown in a). d) The cross-section corresponding to the cut discussed in b). The vertical axis shows the raw signal, indicating a contrast larger than 20%.

Tunneling Microscope (PSTM) [51, 52]. Here the sample is placed on a prism and is illuminated in total internal reflection (TIR). The probe is typically a sharp uncoated fiber tip, and the detector is situated at the far end of the fiber. This setup is often intuitively presented as an optical equivalent of a scanning tunneling microscope in the sense that the photons that would have been otherwise evanescent can tunnel through the glass fiber when it is close. However, the photon tunneling process is usually associated with frustrated total internal reflection between macroscopic bodies [14]. It is more appropriate to talk about scattering when one of the bodies, in this case the tip. has subwavelength dimensions. To this end, we consider PSTM as an apertureless SNOM.

The advantage of PSTM is in its quiet background. The sample is illuminated globally in TIR, and only the signal that is scattered at the junction between the tip and the sample enters the fiber and reaches the detector. The main problem that arises in this mode is that if several nanostructures or edges are illuminated at once multiple reflections of the wave vector component parallel to the surface lead to interferences. The resulting intensity minima and maxima are not representative of the local optical properties of the sample and complicate the image interpretation. Nevertheless, as we will see in sect. 8·2, this method has proven to be quite suitable for mapping the optical

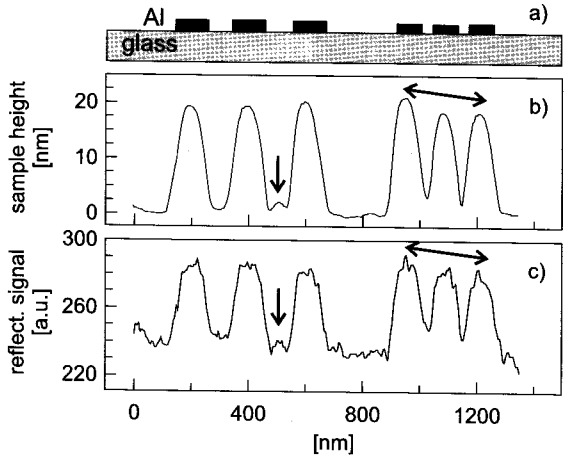

Fig. 18. – a) A test sample consisting of aluminum lines on a glass substrate. b) The topography signal. c) The optical signal when detecting the light coming back into an uncoated fiber tip. The arrows point out to some evident one-to-one correspondence between the two.

intensity distribution in the evanescent field of confined geometries such as waveguides or microresonators [53-57].

6·2. *Uncoated fiber tips.* – Another form of apertureless scanning microscope that also uses an uncoated optical fiber tip and hence belongs to the apertureless family was proposed in 1990. In this mode one illuminates the sample and detects the signal through the same fiber tip [58]. Since there exists no aperture, one obtains 100% transmission (even more than a cleaved fiber since the taper eliminates back-reflections!) which is very attractive when compared to typical transmission of 10^{-5} for aperture probes. It was suggested that in this arrangement the very end of the tip can be taken to act like a small sphere that experiences a near-field interaction with the sample [59], leading to a resolution comparable with the tip curvature. Indeed, first round of experiments reported subwavelength resolution down to 10 nm [58]. However, further studies revealed that the reported ultra high resolution was most probably caused by topography artifacts [43]. It is instructive to take a closer look at these findings because, as discussed in an earlier section, similar problems could appear in other configurations.

Figures 18b) and c) show cross-sections of the topography and optical signals of a test sample (see fig. 18a)) recorded in the internal reflection mode using an uncoated fiber. The tip-sample distance was stabilized via shear-force to a constant gap. Nearly every small detail of the topography comes through the optical image with essentially exactly the same resolution. It is this fact alone that allows one to say with good confidence that the optical signal is an artifact! One has to remember that the shear-force and optical interactions of the tip with the sample stem from two completely different physical origins, and there is no reason for them to show the same resolution.

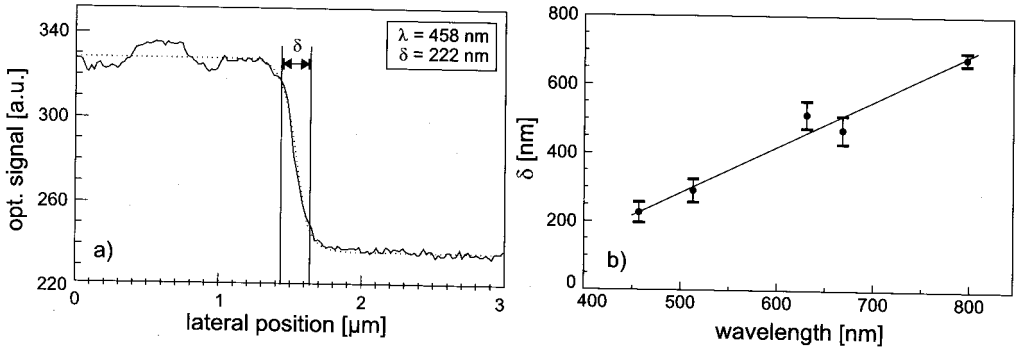

Fig. 19. – a) A typical optical signal when imaging a metal-glass step with an uncoated tip in internal reflection mode. The dotted curve indicates a fit using a hyperbolic tangent [43]. The parameter δ is a measure for the resolution and is plotted in b) when varying the wavelength of illumination through the tip.

In order to examine the imaging mechanism in a more quantitative manner, the edge of a large rectangular aluminum structure on a glass substrate was imaged using different wavelengths of illumination (see fig. 19a)). As shown in fig. 19b), a linear dependence with the wavelength was observed which points to a clear signature of a far-field effect. Further evidence of far-field contributions was also found when the dependence of the optical signal on the tip-sample separation was studied. Figure 20 displays the shear-force and optical signals as the tip was approached to the sample at a fixed lateral location. The oscillatory fringes are created because light that leaks out of the uncoated fiber tip illuminates a diffraction-limited spot on the sample and is then reflected back into the fiber. This field can interfere with residual reflections in the detection system, leading to fringes of fig. 20. After putting all these different parts of the puzzle together one was able to reveal the secret of the imaging mechanism: when scanning the sample, the tip follows its nano-landscape at a constant separation. While doing this the effective phase of the global reflection is modulated according to the sample topography. This results in an optical contrast that possesses a one-to-one correspondence with the topography image and contains no direct information about the local optical properties of the sample.

Although the visibility of the obtained interference fringes is particularly high in the internal reflection mode, some form of multiple scattering or interference is observed in the approach curve of nearly every SNOM. This shows that eliminating far-field contributions is not very easy, and that one has to be quite careful that they do not lead to artifacts. An interesting additional signature of this artifact is the occasional appearance of an inverted contrast. It was not uncommon to perform the same experiment with two different tips and obtain the same resolution but with the reverse contrast. Figure 21 displays an example where the contrast changed in the middle of the scan, most probably because the tip picked up a particle, changing the slope of the interference fringes at the point of contact from negative to positive.

It turns out that an uncoated fiber tip in internal reflection could really be used for

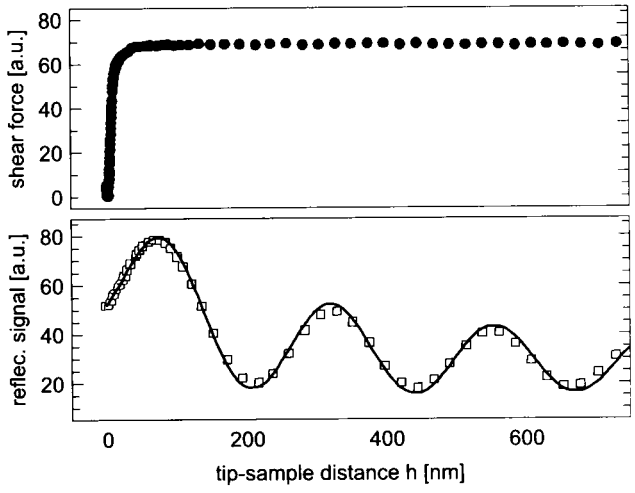

Fig. 20. – Top and bottom curves show the shear-force and optical signals detected when the tip was positioned at different distances z from the sample.

achieving true near-field resolutions if one illuminates with polarized light and detects the cross-polarized light [60]. Here the illumination light undergoes de-polarization when scattered by nanoscopic objects, and the end of the tip picks up this scattering signal and sends it via the fiber through the crossed polarizer onto the detector. Although this technique could in principle provide a good resolution, cross-polarized detection leads to a loss of signal of up to six orders of magnitude, which puts us where we were with the aperture probes.

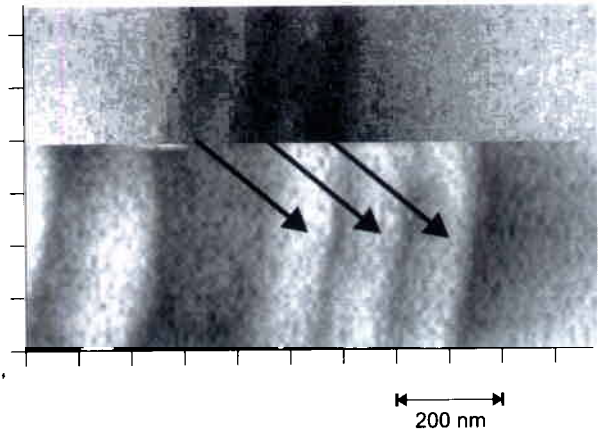

Fig. 21. – An example of contrast inversion in the middle of a scan. Possibly a dust particle was picked up in going from one line to the other, changing the interference conditions in such a way that the slope like the one shown in fig. 20 is changed from negative to positive.

In conclusion, uncoated fiber illumination and detection in its original proposal is not a near-field device. Nevertheless, this configuration could be quite useful for local optical profilometry as well as for a combination of nearly diffraction-limited optical microscopy simultaneous with high-resolution topography imaging [43, 61].

6·3. *Scattering.* – The central idea behind apertureless SNOM is to globally illuminate the combined probe-sample system and locally scatter the high spatial frequency nonpropagating field components from this region. In general one should treat the coupled probe-sample system considering multiple scattering, but often the probe can be considered as a small source of evanescent fields that can be scattered by the sample (fig. 7a)) or as a small detector that locally converts the near fields of the sample into propagating waves (fig. 7b)) [8].

The most important difference to aperture SNOM is that the sample is illuminated globally. From an experimental point of view this causes major problems because of the large background scattering in the system, making the detection of a tiny near-field signal very challenging. To appreciate this point one has to remember that in general the scattering signal is quadratically proportional to the volume. So if we want to examine a particle with a diameter of 3 nm next to another object of 30 nm, the light from the second dominates the signal of interest by about six orders of magnitude. Of course this estimate is quite rough (*e.g.*, completely ignoring the dependence on the dielectric constant and morphology of the sample structures), and is only meant to alarm us about the orders of magnitude. As we will see below, one can play different tricks to discriminate against the background, but the issue of signal-to-noise ratio still remains central in using this mode of SNOM.

The first demonstration of apertureless SNOM was reported by U. Fischer and D. Pohl [62] in 1989 even before conventional aperture SNOM had reached its popularity peak. They overcoated a surface including latex beads with a gold film and excited surface plasmons. The scattering by an individual spherical portrusion in the gold film was used to image a test sample. Specht *et al.* extended this idea and used a metallic tip of a scanning tunneling microscope to image the scattering of surface plasmons on a rough conducting sample [63]. Starting in 1994 three groups [64-68, 44] reported performing apertureless SNOM with dielectric or metallic tips under direct or total internal reflection illumination. The group of K. Wickramasinghe used a silicon AFM tip and chose to illuminate the area around it with a diffraction limited spot. They used the interference between the signal from this region and a second reference beam to directly measure the amplitude of the scattered field. By modulating the tip-sample distance as well as the lateral position of the sample, they implemented a double lock-in technique to separate the near-field signal from the large far-field background. Resolutions down to 1 nm have reported [68], but recent experiments [46, 69] show that the fields reflected from the tip shaft and cantilever lead to interferences and stray signals that also depend on the tip-sample separation (similar to the example of an uncoated fiber tip presented above) and which persist even after lock-in detection. Indeed a careful look at the early published images reveals (too) many instances of one-to-one correspondence between the topog-

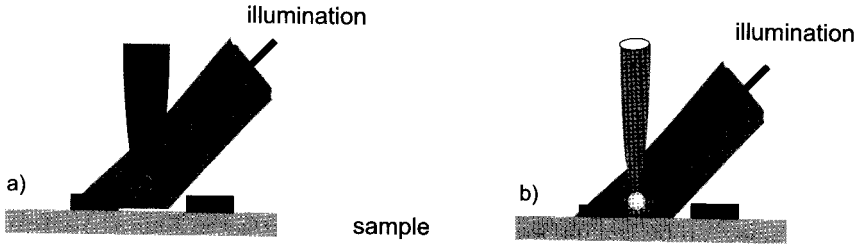

Fig. 22. – a) The general situation of existing experiments using a sharp tip as a probe for apertureless SNOM. The interaction of an imaginary sphere (the white circle) with the sample is often taken as the main source of signal. b) Our approach consists of placing a single gold nanoparticle of well-known size at the end of a glass fiber tip.

raphy and optical images. The suspicion that these first results were strongly affected by topography-induced artifacts together with unfavorable theoretical considerations of the best possible resolution [70] have created a cloud of controversy above apertureless configurations for a few years. Nevertheless, several groups are currently investigating various forms of apertureless SNOM and its limitations [46, 71, 72].

The imaging mechanism in such experiments is often explained via a dipole-dipole interaction between an imaginary sphere at the end of the tip (see fig. 22a)) and the sample features [68, 71, 73]. However, although simplifying an extended tip by a small sphere could be a good start for acquiring some intuition into the problem, a quantitative understanding requires proper consideration of the particle shape and its environment.

In an ideal apertureless SNOM based on scattering a single sphere can be used as a probe [73-75]. The far-field scattering of a sphere with radius a is usually expressed in terms of its scattering cross-section

$$\sigma_{\text{scat}} = \frac{k^4}{6\pi}|\alpha|^2 = \frac{8}{3}\pi k^4 a^6 \left|\frac{\epsilon_1 - \epsilon_m}{\epsilon_1 + 2\epsilon_m}\right|^2 \tag{8}$$

and its absorption cross-section

$$\sigma_{\text{abs}} = k\,\text{Im}(\alpha), \tag{9}$$

where $\alpha = 4\pi a^3((\epsilon_1 - \epsilon_m)/(\epsilon_1 + 2\epsilon_m))$ is the static polarizability of the sphere, and ϵ_1, ϵ_m the complex dielectric constants of the particle and its surrounding medium [76]. For a perfectly conducting sphere of radius $a \ll \lambda$ this result is easy to understand; an incident field $\mathbf{E}_{\text{inc}}$ drives the electrons into an oscillatory motion and induces an electric dipole moment $\mathbf{d} = \alpha\mathbf{E}_{\text{inc}}$ which in turn radiates.

For an oscillating electric dipole $\mathbf{d}$ at the origin pointing in the z-direction the electric

field, magnetic field and the emitted power P can be written in polar coordinates as

$$
\begin{aligned}
E_r &= 2\left[\frac{\mathrm{d}\cos\theta}{r^3}\right](1+ikr)e^{ikr}, \\
E_\theta &= \left[\frac{\mathrm{d}\sin\theta}{r^3}\right](1+ikr-k^2r^2)e^{ikr}, \\
B_\phi &= -\left[\frac{\mathrm{d}\sin\theta}{r^3}\right](ikr+k^2r^2)e^{ikr}, \\
E_\phi &= B_r = B_\theta = 0, \\
\frac{\mathrm{d}P}{\mathrm{d}\Omega} &= \frac{c}{8\pi}k^4\mathbf{d}^2\sin^2\theta, \\
P &= \frac{ck^4}{3}\mathbf{d}^2,
\end{aligned}
\tag{10}
$$

which one usually confronts in the university course on electricity and magnetism [77]. However, their behavior in the near field is usually less emphasized. The chapter by U. Kreibig discusses some peculiarities of the Poynting vector in the near field of a dipolar scatterer. Figure 23 displays the magnitude of the electric field as a function of the angle θ for various distances r. The distribution shown in i) for $r = 10\lambda$ is the familiar far-field radiation pattern of a dipole. As seen in fig. 23b), it rapidly undergoes a substantial change for $r \lesssim \lambda$. The magnitude of the field grows very rapidly as r becomes smaller (note the scales in fig. 23c)-i)). But, more importantly, the ratio between the field strength along the dipole and perpendicular to it reaches a value of 2. In other words, the field reaches its highest value for $\theta = 0$, where it is purely longitudinal. These properties make a dipole moment an ideal SNOM probe due to its extremely large field density in the near field. The existence of a substantial longitudinal field component points to nonpropagating fields with very high frequency Fourier components that can be scattered if an object is brought very close.

In Konstanz we have initiated an experiment where a single gold particle of known size is carefully selected from an ensemble on a substrate and placed at the end of a glass fiber tip (see fig. 22b)) [78]. Figure 24 shows confocal microscope images of a sample with individual colloidal gold particles before (fig. 24a)) and after (fig. 24b)) manipulation with a glass fiber tip. As evident in the electron microscope image of this tip (fig. 24c)), the missing gold particle is attached to its end.

The small dimensions of a sharp glass tip and its low dielectric function of 2.25 compared with $\epsilon = -12 + 1.2i$ for gold (at $\lambda \sim 630\,\mathrm{nm}$) minimize its influence on the scattering properties of the gold sphere. In addition to providing a well-defined and controllable particle size, this probe offers the important advantage of a characteristic spectral response. Figure 25 displays plasmon resonances of two particles of diameters 50 and 100 nm immersed in an oil with an index of refraction of 1.5. Given that a typical sample does not have such a narrow resonance in the visible range, the near-field

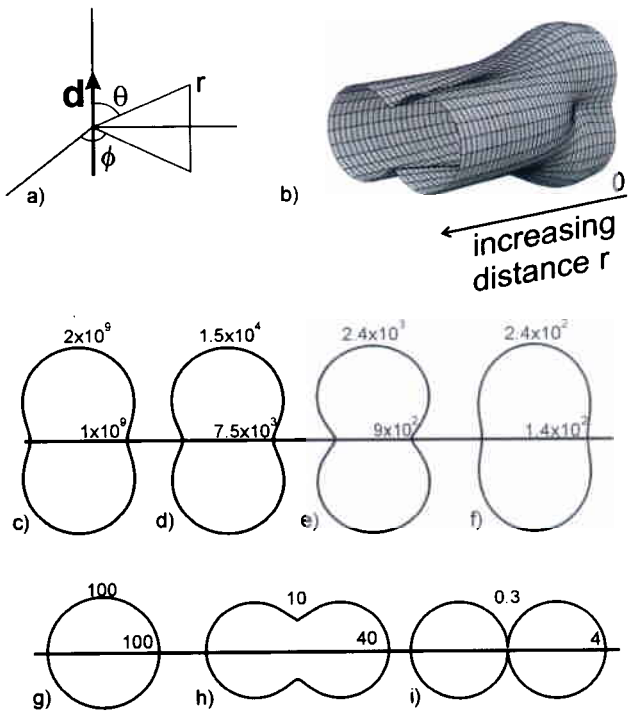

Fig. 23. – a) A dipole d is considered to sit at the origin in the z direction. b) An overview of the electric field at different distances r from the dipole. c)-i) are some cross-sections of this surface for $r/\lambda = 0.001$, 0.05, 0.1, 0.25, 0.375, 1, and 10. The numbers at the axes indicate the magnitude of the field in that direction in arbitrary units.

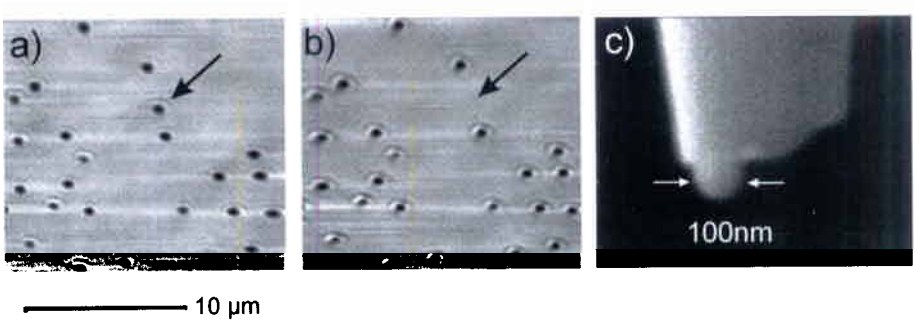

Fig. 24. – a) A scanning confocal image of individual gold particles on a glass substrate before manipulation. b) The same area after picking up one particle. c) An electron scanning microscope image of the probe that was prepared in this manner. The gold particle sits nicely at the end of the glass fiber tip.

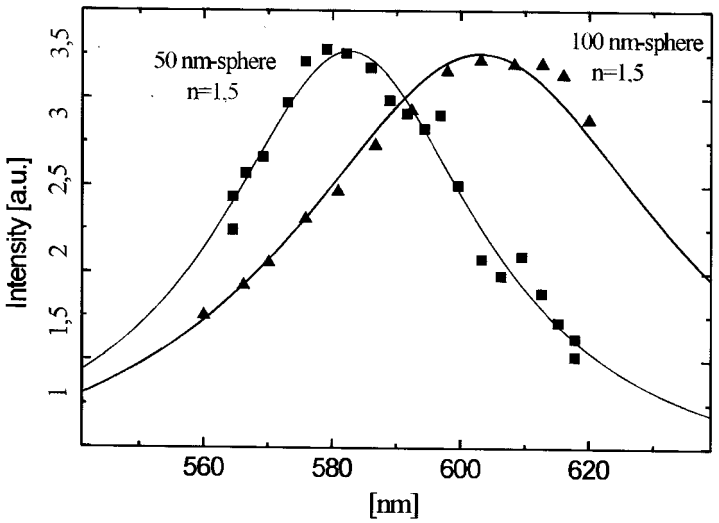

Fig. 25. – Plasmon resonances of two gold particles of diameters 50 nm and 100 nm immersed in a medium with an index of refraction 1.5. The Lorentz fits agree quite well with the predictions of the Mie theory [78].

signal originating from the gold particle could be distinguished from the background light by comparing the signals at two different wavelengths. This spectral selectivity could give a significant advantage over the unfavorable signal-to-background ratio in apertureless SNOM experiments. Another possibility for detection at a wavelength other than the illumination wavelength is generation of the second-harmonic signal (SHG) at the particle [79]. Finally, it is worth noting that a probe such as that in fig. 24 holds important promise for *in vivo* three-dimensional near-field imaging of biological samples.

6·4. *Antenna effects.* – We have already pointed out that, unless one manipulates a single scattering particle as a probe, the geometry of the tip plays an important role in imaging. Simple treatments of an extended sharp probe consider an ellipsoid or a cone. Scattering from an ellipsoid can be solved analytically in a similar manner to Mie scattering from a sphere. In the general case of different axes $a \neq b \neq c$ one can induce three dipole moments with polarizabilities

$$\alpha_i = 4\pi abc \frac{\epsilon_1 - \epsilon_m}{3[(\epsilon_1 - \epsilon_m)L_i + \epsilon_m]} \tag{11}$$

for a field parallel to the i-th axis [76]. Here L_i are geometrical factors that depend on a, b, and c and which satisfy the sum rule $\sum L_i = 1$. For a spheroid of $b = c$ and very large a, *i.e.* a needle-shaped structure, L_a approaches zero and the polarizability becomes $\alpha_a = 4\pi abc((\epsilon_1 - \epsilon_m)/3\epsilon_m)$. For a glass spheroid elongation of one axis only leads to

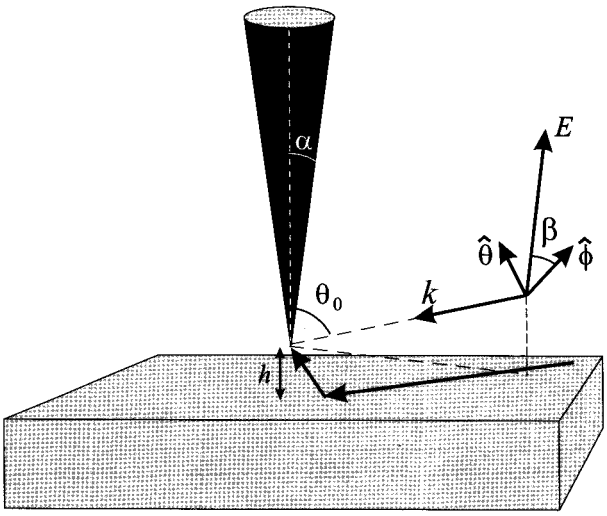

Fig. 26. – Schematic representation of a cone near a dielectric surface illuminated at an arbitrary angle.

scattering one order of magnitude larger than that of a sphere. However, combination of the geometrical effects and plasmon resonances in metals could give rise to an up to three orders of magnitude increase in the scattering coefficient [80]. Such enhancements in the polarizability mean correspondingly larger dipole moments and larger near fields that are well localized to the region of high curvature, namely the tip. Due to its analogy with the function of a lightning rod, this field enhancement is often referred to as the lightning rod effect.

A more realistic model for apertureless SNOM with a tip is obtained when considering a cone. For a plane wave incident on a perfectly conducting cone the scattered field can be calculated analytically for the near-field region $kr \ll 1$ [81] and can be written as

$$\mathbf{E}(\theta_0, \beta) \cong (kr)^{\nu-1} \sin(\beta) \left(\hat{\mathbf{r}} + \frac{1}{\nu} \hat{\theta} \frac{\partial}{\partial \theta} \right) a(\theta_0, \theta, \alpha), \tag{12}$$

where angles θ_0, β, θ, α are as defined in fig. 26. The parameter ν is a constant smaller than unity and depends on α, whereas r indicates the distance of the observation point from the apex of the cone and a is a function of θ_0, θ and α [72]. Cory *et al.* have also considered the effect of a dielectric surface in the vicinity of the tip by taking into account the reflection of the field from the surface [82]. One of the most important aspects of this result is that for s-polarized illumination ($\beta = 0$) the electric field vanishes as demonstrated experimentally in [72]. Note that this is neither the case for a sphere nor for a finite-sized ellipsoid and is a consequence of the extended nature of the cone which acts as an antenna that picks up a certain polarization. Despite its super-wavelength dimensions such a cone can be used for apertureless SNOM with very high resolution.

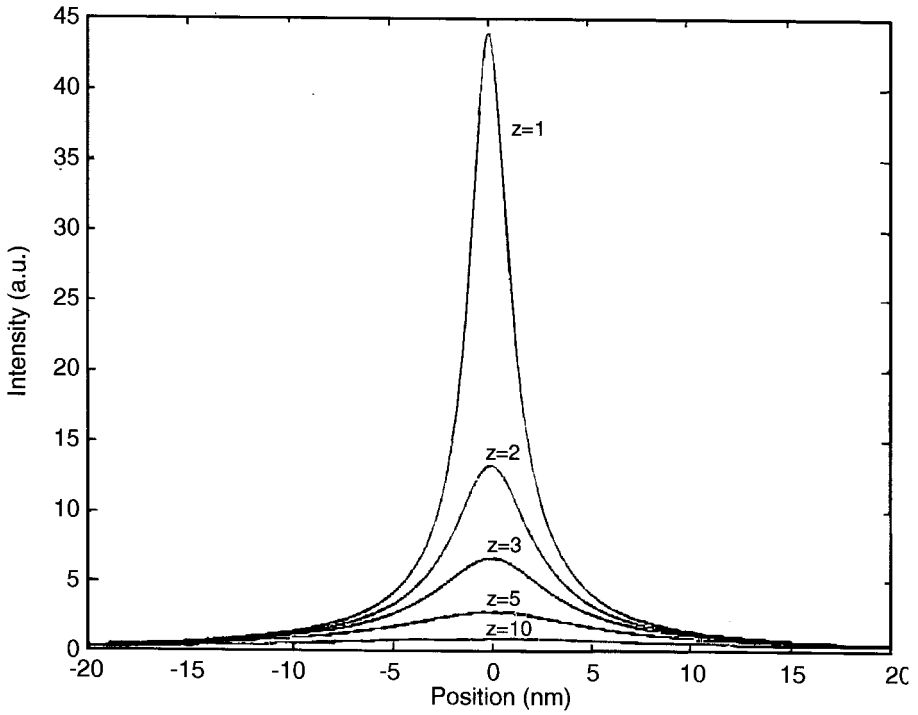

Fig. 27. – Field intensities at different separations z from the tip of the cone. $\alpha = 3°$, $\epsilon_r = 2.4$ and $\theta_0 = 100°$ (taken from [82]).

Figure 27 shows the lateral extent of the intensity in observation planes at different distances from a very sharp tip. For very small separations under 5 nm the optical field is concentrated in a very small lateral region of a few nanometers. This confinement improves as the tip becomes sharper, but the degree of field enhancement decreases so that for practical purposes a compromise would have to be reached. Finally we note that scattering from such a sharp tip displays a specific wavelength dependence that is determined by the shape of the tip and which, contrary to the case of Rayleigh scattering, increases with increasing wavelength [83].

The strong confinement of the electromagnetic energy in the immediate vicinity of the tip apex can be used to interrogate the sample very locally. It has been pointed out by several groups [79, 80, 84, 85] that this phenomenon could be particularly useful for studying nonlinear optical processes. Indeed a recent experiment has demonstrated two-photon excitation of fluorescence using a very sharp gold tip [86]. The intensity enhancement was estimated to be of the order of 1000 but due to the second-order nature of the process an enhancement up to 10^6 could have contributed to the excitation of photosynthetic membranes. Another recent experiment has reported application of field enhancement at a sharp tip for Raman spectroscopy [87]. The idea of exciting Surface-Enhanced Raman Spectroscopy (SERS) using a sharp tip is very appealing because in

this manner one could introduce the same geometrical roughness (*i.e.* the tip) to different parts of the sample and perform controlled experiments that might reveal the secrets of SERS.

Instead of using the strong fields for studying nonlinear processes of the sample, one could also exploit nonlinear signals created at the tip to perform SNOM. The idea here is similar to that mentioned earlier with regard to SHG signal from gold particle probes. Covering a sharp tip with nonlinear active molecules is another way of creating a very localized light source at a wavelength other than the illumination [79]. The next section will pursue other ideas in the category of nanoscopically confined light sources.

7. – Apertureless SNOM with active probes

So far we have considered a) local illumination of the sample via the evanescent fields of an aperture and b) global illumination of and local scattering from the sample-probe system. We now take a look at the idea of a fluorescent nanoscopic probe as shown in fig. 28. Here the sample-probe system is illuminated globally at wavelength λ_{exc}. The probe absorbs this light and emits at a wavelength λ_{em} which is used for near-field illumination of the sample. In practice the emitted intensity of such a probe is not constant if the medium is excited below saturation. This is because due to scattering from local sample structures the intensity of the excitation light is also modulated while the sample is scanned. However, as we will see shortly, this complication is removed if one monitors the modification of the molecular spectrum instead of its emission intensity.

Similar to a scattering probe a nanoscopic active probe has the advantage that its size can be reduced to an arbitrarily small size. In the scattering scheme the signal scales as a power law of the volume and rapidly drops below the background as the probe is made smaller. However, using very efficient fluorescent material that emits at a wavelength λ_{em} different from λ_{exc} one can obtain a healthy signal down to the single-molecule level. So contrary to the scattering case, in this mode of operation the signal-to-noise ratio is not a determining factor in the attainable resolution.

In a first intuitive approach one immediately draws the analogy between nanoscopic emitting probes and that of an aperture probe where the light exiting the subwavelength opening has been replaced by the emission from a subwavelength source. Below we will see that although this view takes us a long way, the internal structures of emitting atoms or molecules have to be taken into account and can even be used for novel types of imaging.

7·1. *Radiation from a single dipole moment.* – The most elementary building block of a fluorescent medium is an atom or a molecule. An atom or a molecule is often treated as a classical dipole moment with a certain resonance frequency, linewidth and amplitude. This simplification has been extremely successful not only in providing intuition into many aspects of the less graspable quantum-mechanical world of atoms, but also in the quantitative description of several atomic and molecular processes (aside from an occasional factor of 2 discrepancy [88, 89]). In what follows we will restrict ourselves to

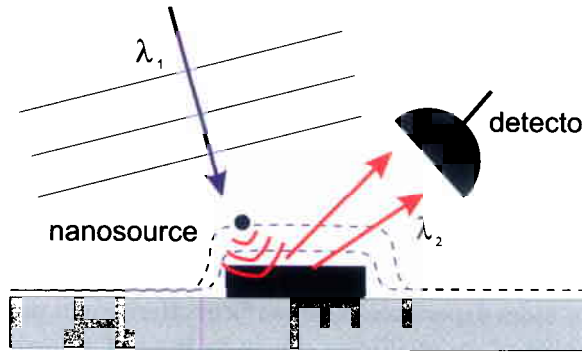

Fig. 28. – Schematic view of an active medium excited in the immediate vicinity of the probe. The strength of the field at the location of the molecule could strongly depend on the sample.

this approach because it turns out that it is particularly robust in the near field [89].

Before we treat the problem of such a dipole in front of a sample in more detail, let us address a question that might seem puzzling at first. We know that when we excite an atom it decays after a short time and emits a photon that can be detected in the far field. So given this propagating emission, how could one talk about evanescent waves and near-field imaging? Formulated in another way, how could one confine photons from an atom or molecule to a nanoscopic region necessary for ultra high resolution microscopy? The answer to the question lies in that any emitted photon field has to undergo the same evolution as in fig. 23, *i.e.* from a longitudinal character to a transverse propagation one. Let us emphasize that having a real quantum-mechanical atom or a classical dipole does not make any difference because in a quantum-electrodynamical treatment of the field around an atom one finds exactly the same radiation pattern as in the classical case [90]. Of course once a free atom in the excited state emits a photon and returns to the ground state, there are no near fields any more. But if we keep exciting it, there is always a near field present that can couple to the sample. As you see in the next section, however, this coupling is not negligible and could strongly change the atomic emission spectrum and pattern.

7˙2. *Interaction of a dipole with a flat surface.* – The radiative properties of an atom in the vicinity of a flat perfect mirror can be handled in a fairly straightforward manner using several different approaches [90]. There have been quite a few discussions on whether or not one needs to invoke a full quantum-electrodynamical treatment. Although the general case of an atom placed at an arbitrary location in front of a mirror is best described by such a theory [89], an atom in the near field of a surface can be treated quite accurately with a classical approach as shown for example by Chance, Prock, and Silbey (CPS) [91]. In this point of view one replaces the atom with an oscillating electric dipole moment that is driven by an electric field $\mathbf{E}_{\mathrm{loc}}(\mathbf{r})$ at its location $\mathbf{r}$ and accounts for spontaneous

emission by a phenomenological damping rate γ:

$$\mathbf{d}'' + \gamma(\mathbf{r})\mathbf{d}' + \varpi_0^2\mathbf{d} = \frac{e^2}{m}\mathbf{E}_{\rm loc}(\mathbf{r}), \tag{13}$$

where $\mathbf{E}_{\rm loc}(\mathbf{r}) = \mathbf{E}_{\rm dip}(\mathbf{r}) + \mathbf{E}_{\rm ref}(\mathbf{r})$ represents the field of an unperturbed dipole and the field that is produced after reflection or scattering from the boundaries. We will not discuss the subtleties and limitations of any particular models here and refer the interested reader to the specialized literature [92, 90, 93]. Figure 29 gives a flavor of the modifications that an atom experiences near surfaces. Here we have plotted the lifetime and the frequency shifts of an oscillating dipole in front of a perfectly reflecting and infinite mirror calculated according to the CPS model. The two important aspects of the interaction, namely its dependence on the orientation of the dipole moment and on the distance, are clearly emphasized. Both in figs. 29a) and 29b) one observes oscillations for larger distances which can be understood as the consequence of the propagation phase of the dipole field reflected from the mirror. In the near field the level shifts simply obey the Lennard-Jones potential and vary as d^2/z^3, where d is the electric dipole moment and z the distance to the surface [94].

Such classical calculations have been very successful in describing the experimental observations made on the modification of the lifetime near realistic surfaces as pioneered in the sixties by Drexhage [95]. In particular they can even show that in the near-field region, $z \ll \lambda/2\pi$, the high spatial frequency components of the dipole radiation can couple to surface modes such as surface plasmons in metals or to lossy surface waves excited by the oscillations of electronic charge density. Due to nonradiative broadenings of resonances, experimental verification of the energy level shifts is usually not possible in adsorbate systems. A few examples of studies on free atoms close to surfaces (but not very close) or on organic spacers can be found in refs. [96-98].

In addition to the modification of the dipole's internal structure such as its linewidth or resonance frequency, the presence of a surface heavily influences its radiation pattern [99, 100]. Figure 30 displays radiation of a dipole placed in the near field of dielectric or metallic substrates either perpendicular or parallel to the surface. Particularly interesting is the coupling of the dipole emission into angles larger than the critical angle. This is most pronounced for a perpendicular dipole moment since its emission in free space has a substantial component parallel to the substrate. On the other hand, the emission pattern of a parallel dipole has become somewhat asymmetric, but as in free space most of the emission still propagates normal to the dipole orientation. In the case of a metallic film the presence of surface plasmons plays a decisive role.

7·3. *A dipole in front of a structured surface: optical microscopy with vacuum photons.* – Typical surfaces in the laboratory are not very flat on the nanometer scale, and surface roughness has been known to influence the emission properties of emitters in the vicinity [93]. In the context of SNOM it is interesting to study the effect of small nanostructures on the emission characteristics of a dipole moment. Here too one would like to know the effect of the local structure on the emission lifetime, resonance frequency

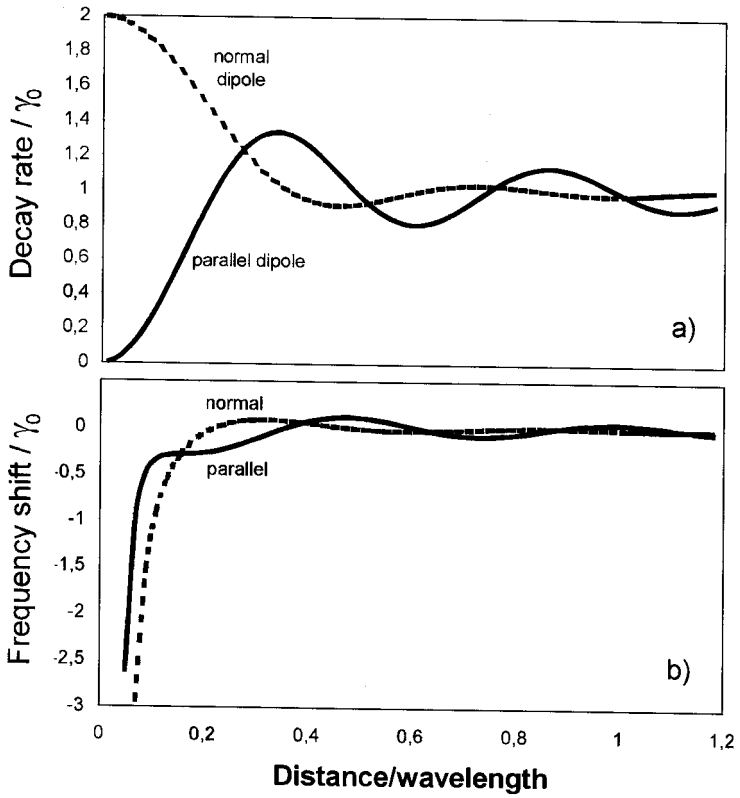

Fig. 29. – a) Modulations of the fluorescence lifetime of an emitter as a function of its distance to a perfect mirror for normal and parallel dipole orientations. b) Same as a) but for the frequency shift.

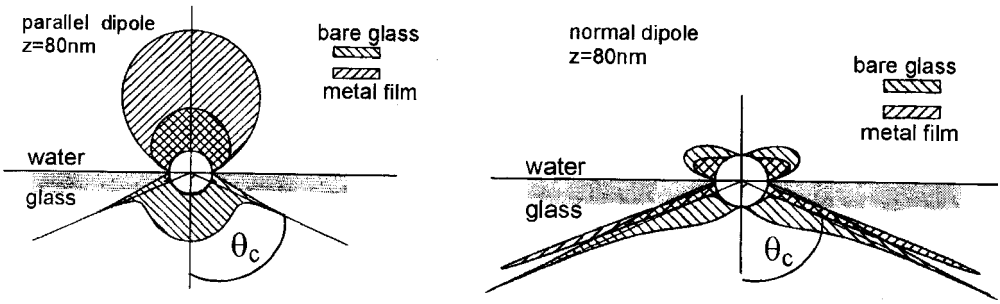

Fig. 30. – The radiation pattern for dipoles oriented parallel and perpendicular to an interface between two media, either water and glass or water and metal-coated glass. Taken from [100].

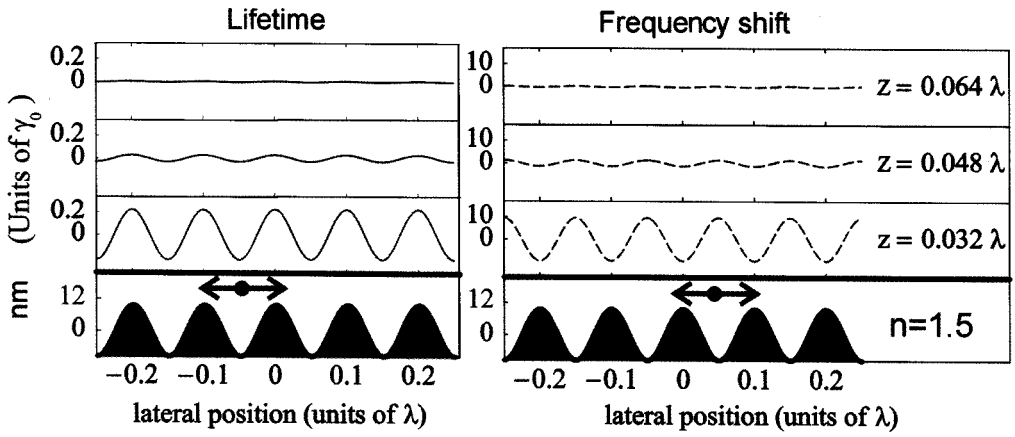

Fig. 31. – Modulations of the lifetime and lineshift of a dipole moment placed at different heights and scanned in front of a phase grating made of glass [107]. γ_0 indicates the linewidth of the unperturbed dipole.

as well as radiation pattern. Indeed experiments have shown that the presence of a conventional aperture SNOM tip leads to the modification of the fluorescence lifetime of molecules placed on a dielectric substrate [101, 102]. Particularly interesting is that this modification depends very strongly on the very local environment, for example the metallized part or the glass part of the probe.

From the point of view of calculations this demands new techniques because the existing analytic methods such as the CPS model, which relied on matching the boundary conditions for the fields at flat interfaces, do not work anymore. Several authors have gained some insight into the modification of the fluorescence lifetime using numerical techniques [103-106]. Although for arbitrary geometries one cannot get around numerical calculations, analytic approaches with approximations provide more valuable intuition [107, 108]. One such approach is to Fourier decompose a rough surface into a sum of sinusoidal gratings and then use a Green function formalism to calculate the i-th component of the reflected field $\mathbf{E}_{\mathrm{dip},i}(\mathbf{x}) = \sum_j G_{ij}(\mathbf{x}, \mathbf{r}; \omega)\mathbf{d}_j(\mathbf{r})$ at position $\mathbf{x}$ if the dipole sits at position $\mathbf{r}$. One can then arrive at the modifications of the frequency shift and linewidth [109, 110] according to

$$\frac{\delta\omega_j(\mathbf{r})}{\gamma_0} - \frac{\mathrm{i}}{2}\frac{\gamma_j(\mathbf{r})}{\gamma_0} = -\frac{3\pi\varepsilon_0}{k_0^3} G_{jj}(\mathbf{r}, \mathbf{r}; \omega_0). \tag{14}$$

In this treatment we limit ourselves to the approximation of soft corrugations. This allows us to linearize the surface profile and separate the contribution of the surface roughness (first order in the approximation) from that of the flat component of the substrate (zeroth order). Figure 31 shows the first-order contribution to the lifetime and frequency shift as the molecule is scanned across a shallow glass grating at different

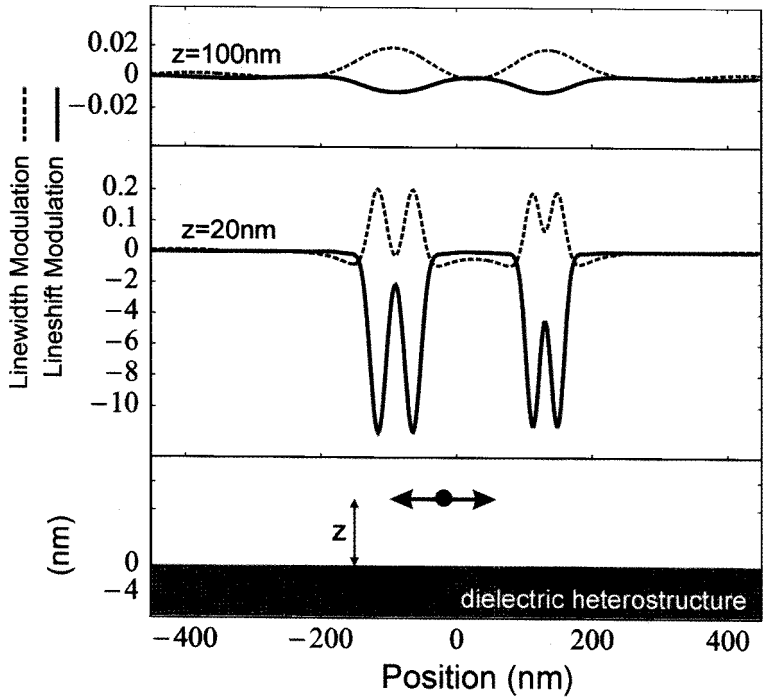

Fig. 32. – Modulations of the lifetime (dashed lines) and lineshift (solid line) of a vertical dipole scanned in front of a dielectric heterostructure [107]. The index of refraction of the substrate is 1.5 and of the nanostructures 2.5.

heights. The observed modulations mirror the roughness of the sample very well, showing that the spectral properties of an emitter are very sensitive to small nanoscopic changes.

Having treated a phase grating, one can then perform these calculations for general dielectric samples with lateral nanostructures in the topography or in the index of refraction. Figure 32 shows the results for the linewidths (solid lines) and lineshifts (dashed lines) at two different separations from a dielectric topography-free sample. First, we note that in both cases the structures are well resolved when the molecule is close but washed out when the molecule is farther away. This is the familiar sensitivity of the resolution on the probe-sample separation that one expects in SNOM. Furthermore, as expected for a point-like source, the obtained resolution is of the order of the separation between the molecule and the sample. The images obtained from the lineshift are more representative of the sample structures than those obtained from the linewidth (note the overshoots in the solid lines), and also the size of the lineshift modification is more pronounced. This was not noticed before, and in fact the modifications of the lineshift are usually believed to be too small to be measured. We will see below that we might be close to the experimental demonstration of these effects using a single molecule. Finally, we emphasize that the measurable signal in this imaging mode comes from the internal

structure of the molecule and is therefore independent of the illumination or detection channels. In fact, to the extent that the radiative properties such as spontaneous emission are, strictly speaking, of quantum electrodynamic origin, this imaging mechanism also has its roots in probing the local variations of the vacuum field fluctuations. In other words, the information about the optical properties of the sample is propagated via virtual photons that are scattered by the nanoscopic structures on or in the substrate.

Using this analytic method [111] or numerical calculations [105] one can also study changes in the dipole radiation pattern as it is placed close to a nanostructure. Very recently such modifications of the radiation pattern were also demonstrated experimentally using an aperture SNOM tip and a single molecule [112].

7·4. *Finite-size sources.* – Assuming that a fluorescent probe can be brought to the immediate vicinity of the sample, we need to meet three important requirements. First, the active medium has to be located at the very end of the probe. Second, the depth of this medium has to be much smaller than its lateral dimensions. Finally, the fluorescent material has to be very bright and photostable. These requirements have turned the goal of probe preparation into a very challenging task.

The literature on the use of fluorescent media as probes for SNOM dates back to 1990. The first work related to this idea reported on filling a metal-coated pulled hollow pipette with a molecular crystal that could be excited in the near ultraviolet and emitted in the blue [36]. This idea was also extended to pipettes filled with fluorescent polymers [113, 114] or an electroluminescent powder [115]. In all these, however, since the depth of the material in the pipette was substantially larger than a wavelength, an aperture was used to confine the light. To this end, the resolution obtained in this approach is still governed by the size of the aperture and was about 200–300 nm.

There have been several other activities and ideas regarding the use of different active material as well as approaches to a controlled probe fabrication. Kurihara *et al.* [116] carefully dipped a fiber tip into a solution of Rhodamin 6G contained in a small capillary. After the solution had evaporated the dye molecules sedimented onto the tip, but it was difficult to fine-tune this method and prevent the material from running up the fiber. Stürmer *et al.* have reported a microfabrication method whereby a very thin layer of dye-doped polymer is coated on a polymer substrate [117]. Using the proper mask, the whole sample is then etched to fabricate a plastic AFM cantilever in such a way that the thin fluorescent part is at the very end of the tip. In Konstanz we have also developed a method that shows particular promise for the fabrication of probes with fluorescent media of dimensions under 50 nm positioned at the very end of a dielectric probe [118]. First we spin coat a solution of a polymer that is doped with the desired fluorescent material onto a silanized substrate. Then the sample is heated to induce dewetting and formation of small droplets. After having imaged the topography with an uncoated pulled tip we heat the substrate *in situ* and dip the tip into a soft droplet. By choosing the appropriate droplet, we can predetermine the size of the active medium. Figure 33 shows an electron microscope image of such a probe. Other efforts in this direction have concentrated on the use of porous silicon [119], nonlinear crystals [120] or color centers [121] as emitter,

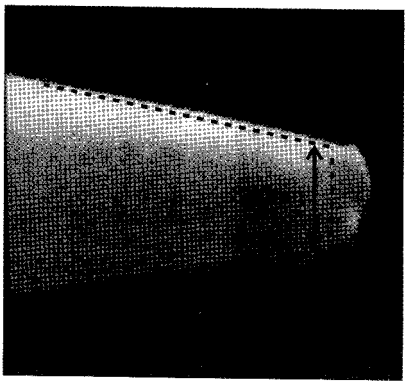

Fig. 33. – An electron microscope image of a tip with a small amount of polymer at its end. The dashed lines show the contour of the tip prior to the placement of the polymer droplet [118].

but media such as semiconductor quantum dots [122] and light-emitting polymers could also be suitable candidates.

So far none of these methods have succeeded in meeting all the three requirements mentioned above. For example the method used by Kramper *et al.* in principle solves the problem of controlled probe fabrication [118], but has suffered from the limited signal due to photobleaching of dye molecules. On the other hand, the color centers in [121] seem to be extremely photostable, but their integration at the end of a sharp probe has confronted problems. Nevertheless, it is reasonable to believe that these technological barriers can be removed in the near future. In particular, a battery-operated electroluminescent SNOM probe using a semiconductor quantum dot source could offer an elegant avenue for optical near-field microscopy.

7·5. *Single-molecule source.* – Despite the fact that the demonstration of SNOM with active probes of finite subwavelength dimensions has not been satisfactory, several groups have pushed this idea further and have proposed the use of a *single* molecule or atom as a light source [107, 123-125]. In this arrangement one expects to reach a molecular resolution in optical microscopy if this molecule could only be brought to comparable separations from the sample. Progress toward optical detection of single molecules has advanced somewhat parallel to that of SNOM. Over more than a decade many groups have demonstrated and used single-molecule detection and spectroscopy in a wide variety of experiments [126]. We discuss here very basic essentials of single-molecule detection so the reader gets a feeling for it.

In 1989 the first report of optical spectroscopy on a single molecule in a solid matrix was published by Kador and Moerner [127]. Here an organic crystal doped with impurity molecules was cooled down to temperatures under 2 K so that the homogeneous linewidths of the individual molecules were reduced to their natural linewidth limits of the order of 10 MHz (about $0.001\,\mathrm{cm}^{-1}$ or $0.1\,\mu\mathrm{eV}$). By choosing a doping concentration of about 10^{-6} and taking advantage of the inhomogeneous distribution of molecular res-

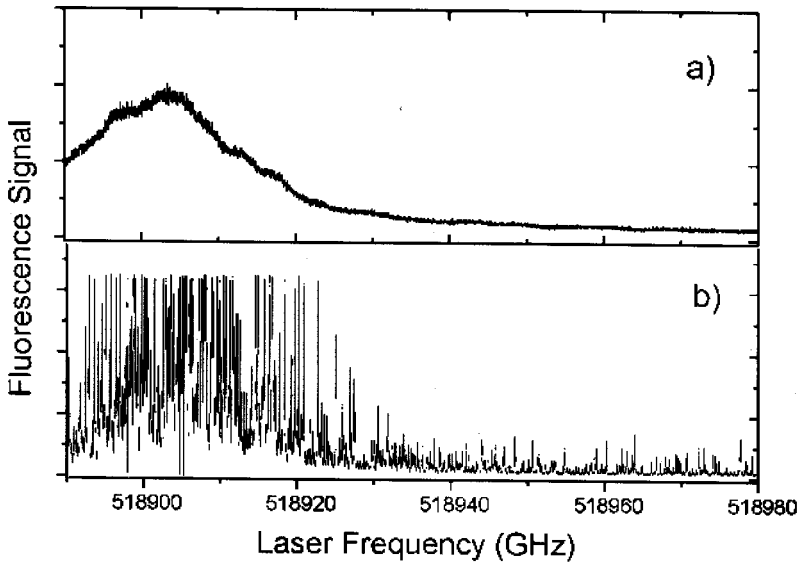

Fig. 34. – a) Spectrum of a weakly doped terrylene in p-terphenyl at room temperature. b) Same as in a) but at $T = 1.4\,\mathrm{K}$. Some of the signal is truncated due to detection saturation. Individual lines in b) represent fluorescence from individual molecules.

onances in a solid matrix, one could find regions of the absorption spectrum where the spectra of different molecules did not overlap (see fig. 34). The first experiments were done by directly detecting the absorption of a single molecule, which meant measuring a very small dip in a large signal. To appreciate this, let us consider some orders of magnitude. A single molecule of linewidth 10 MHz can at best emit about 10^7 photons per second, yielding a count rate of about 10^5 if assuming a realistic overall detection efficiency of 1%. If the required laser power is about $100\,\mathrm{nW} \sim 2 \cdot 10^{12}$ photons per second, the shot noise on the laser signal would be itself about 10^6 counts per second, which is comparable with or larger than the expected count rates. This is why even after using lock-in techniques the obtained signal-to-noise ratio was not very high. A year after this discovery Orrit and Bernard showed that one would achieve a much better signal-to-noise ratio if one detected the Stokes shifted fluorescence of a single molecule [128]. Since this is at a different wavelength than the excitation, one can use good spectral filters to reduce the background essentially to zero.

In 1993 individual molecules spread on a surface were also detected using SNOM at room temperature [31]. This was a breakthrough because at room temperature the absorption cross-section of dye molecules is substantially smaller, which means that one has to use higher excitation powers. This in turn leads to fluorescence from almost everything else in the optical path, such as the optical fiber, remaining solvent on a substrate, optical filters, etc. So the idea behind using a SNOM was to reduce the

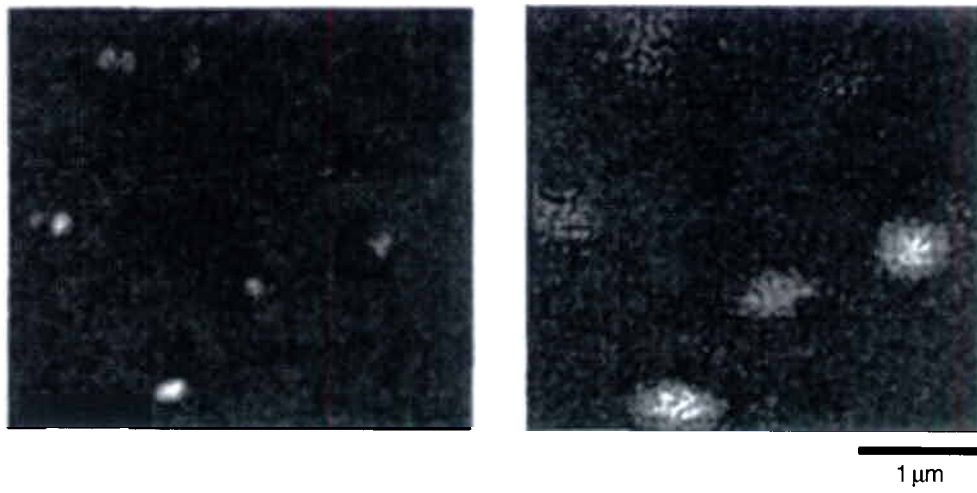

Fig. 35. – Left is a fluorescence image of single molecules using SNOM and the right-hand side displays a confocal image of exactly the same area. Taken from [130].

illumination spot such that one minimizes the background while also gaining spatial resolution. Soon after this first demonstration other groups succeeded in detecting single molecules also in a confocal arrangement [129], with the advantage of being faster, easier and having a larger signal-to-noise ratio. Figure 35 compares two images taken from the same area of a sample using SNOM and confocal illuminations [130] showing that, nevertheless, the resolution in SNOM is clearly superior.

In these experiments a single molecule is illuminated for a total time of about a few hundreds of milliseconds. However, a single-molecule probe has to deliver a reasonable signal for a long time if one wants to perform reproducible measurements. It turns out that adsorbed molecules or those embedded in very thin films are not very photostable. A typical estimate for the life of a fluorescent molecule is believed to be between 10^6 to 10^8 emitted photons at best before it bleaches [131]. Therefore, if we require a count rate of 10^3–10^4 Hz for a comfortable detection and again assume a detection efficiency of 1%, one could do an experiment with a single molecule up to maximum of 20 minutes. It is also interesting to mention that even during their lives many single-molecule systems show "blinking", which is an intermittent on-off effect, not yet fully understood [132]. The duration of the off-time could range between microseconds to tens of milliseconds, making imaging less straightforward. Admittedly these considerations are very loose, and one can win or lose factors of 2 at many places. Nevertheless, the final message remains valid that today at room temperature all molecules are unsuitable as a probe for SNOM. There are many efforts, however, to improve the photochemistry of emitters in order to overcome these problems.

In addition to a successful optical detection of single molecules, performing SNOM with a single-molecule probe requires proper handling and positioning. Naively, one

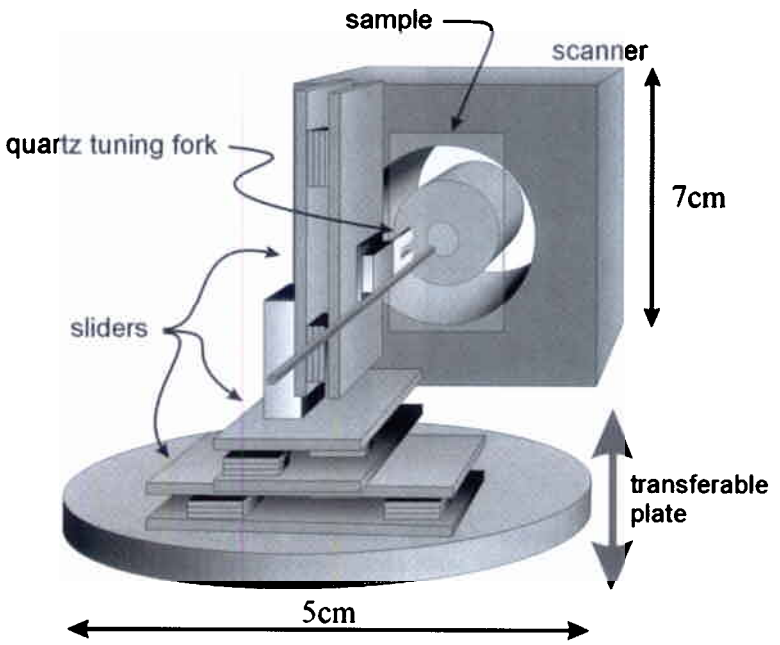

Fig. 36. – The schematics of the cryogenic SNOM/confocal microscope. The probe as well as the microscope objective can be positioned against the sample by home-made piezo-driven translation stages (sliders). The sample can be scanned using a commercial piezo scanner. A quartz tuning fork is used to perform shear-force stabilization of the distance between the probe and the sample.

could imagine dipping a fiber tip into a solution that contains a low concentration of dye molecules and hope that some would stay at the front. Although someone might have a clever way of making this work, the probability of having a single molecule exactly in the last few tens of nanometers is very low, making a practical experiment nearly impossible. Another thought that might come to mind is mechanical manipulation and placement of a single molecule at the end of a fiber tip in a manner similar to the works of D. Eigler or J. Gimzewski [1, 2]. Despite its complexity, this avenue could possibly work but has not been tried yet. Finally, Letokhov and coworkers are planning to use a field emission diagnostic to locate individual color centers in a crystal at the end of a tip [124].

In Konstanz we have recently succeeded in realizing a scheme that has allowed repeated measurements with a single molecule as a light source for optical microscopy [133]. Our approach was to attach a microscopic para-terphenyl crystal that is doped with terrylene molecules at the end of a fiber tip. We then applied the method of fluorescence excitation spectroscopy [128] discussed earlier to select one single molecule in frequency space. This experiment took place at a temperature of 1.4 Kelvin in a cryostat using a combined SNOM/confocal device with a quartz tuning fork, piezo-electric scanner, coarse positioners and a microscope objective, [134] as shown in fig. 36. Although technically

quite a bit more demanding than a room temperature experiment, the photostability of single molecules in this scheme fully compensates for the trouble one has to go through. Figure 37 shows images taken with the same single molecule at different separations from the sample which consisted of 25 nm thick aluminum triangles on glass. Each image was taken in about 25 minutes while the total duration of the experimental run was about 4 hours. The photostability of the molecule, the thermal and mechanical stability of the system, as well as the reproducibility of the imaging process are all quite evident when comparing these images.

The individual metallic islands are clearly distinguishable in all four fig. 37a)-d), but as the substrate is brought closer to the molecule the images become sharper and the resolution is improved. Particularly interesting is the image of the area around a defect in the sample (see the arrow in fig. 37e)) which only becomes clearly detectable at the lowest tip-sample separation. Nevertheless, the triangular geometry that one would have expected naively for each island is not visible in any of the images. Instead, each figure shows different patterns of dark and bright regions that are very reproducible within that image. In particular, in each figure one finds two different shapes of islands that correspond to the differently oriented islands labeled *i* and *ii* in the topography image (see fig. 37e)). All these properties are also found by preliminary numerical simulations [135] where the emission of a dipole oriented in the x, y, or z directions is propagated through the sample. These results are displayed in fig. 38 for two different distances between the molecule and the sample. The qualitative outcome of the images for different dipole orientations is remarkable. The modulation of the signal close to an aluminum island has also been encountered in theoretical and experimental works in conventional SNOM imaging when polarized light was used for illumination [38-40]. In our case a quantitative comparison of calculations with the experimental results could reveal the dipole orientation in the crystal.

Although the images shown in fig. 37 seem very robust and agree with the simulations in a qualitative manner, a molecular resolution which one might have hoped for is definitely not the case. This is not surprising though since the dye molecule sits well inside the microcrystal and the given separations in fig. 37 only specify the distance of the sample from the crystal's end edge and not from the molecule itself. Work is under progress to control the production and size of the crystal at the end of the tip. This will automatically lead to the detection of molecules that are minimally distanced from the ultimate extremity of the crystal edge. Needless to say, it would be particularly interesting to access molecules that lie within the last 2–5 nm of the crystal. Such an arrangement would make it possible to image secondary individual fluorescent molecules on a substrate via Fluorescence Resonance Energy Transfer (FRET) [136, 137] between the probe molecule and a sample molecule. The basic mechanism of FRET relies on the dipole-dipole coupling between a donor and an acceptor molecule. If the emission frequency of the donor matches that of the acceptor absorption, one can imagine that the donor emission and the acceptor absorption dipoles couple in a resonant manner, leading to the transfer of energy from one to the other, quite similar to the case of coupled harmonic oscillators. For an efficient transfer of energy several conditions have to be

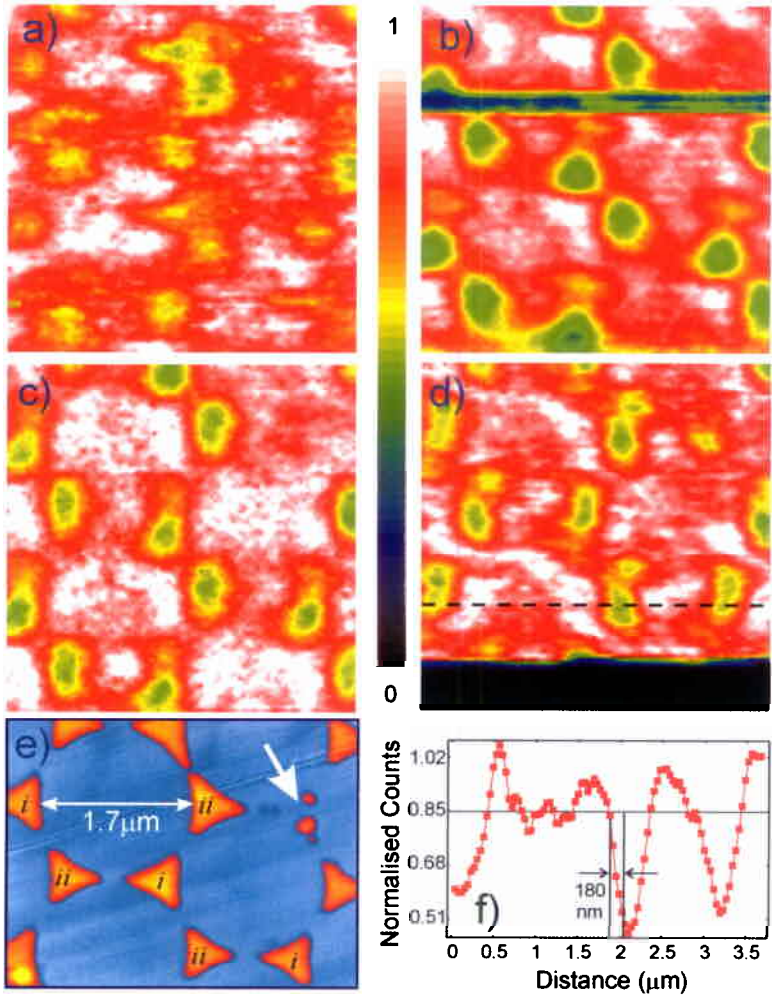

Fig. 37. – Images taken with a single-molecule probe at different separations from the sample. a), b), c) and d) show cases where the edge of the crystal was placed at 350 nm, 80 nm, 50 nm, and 20 nm from the sample surface. e) An AFM image of the section of the sample where the measurements were done. f) A cross-section from d) is displayed.

met: a good spectral overlap, proper orientation of the dipole moments and a very small separation R between the donor and acceptor. In practice the latter condition is the most important of all since the transfer rate scales as $(R_0/R)^6$ with R_0 being the distance at which the rates of the FRET and decay via spontaneous emission are balanced.

A few other groups are currently working to demonstrate a FRET-SNOM [138] at room temperature. The approach here is to place a finite amount of a thin film containing acceptor molecules at the end of a tip and scan it against a substrate that contains

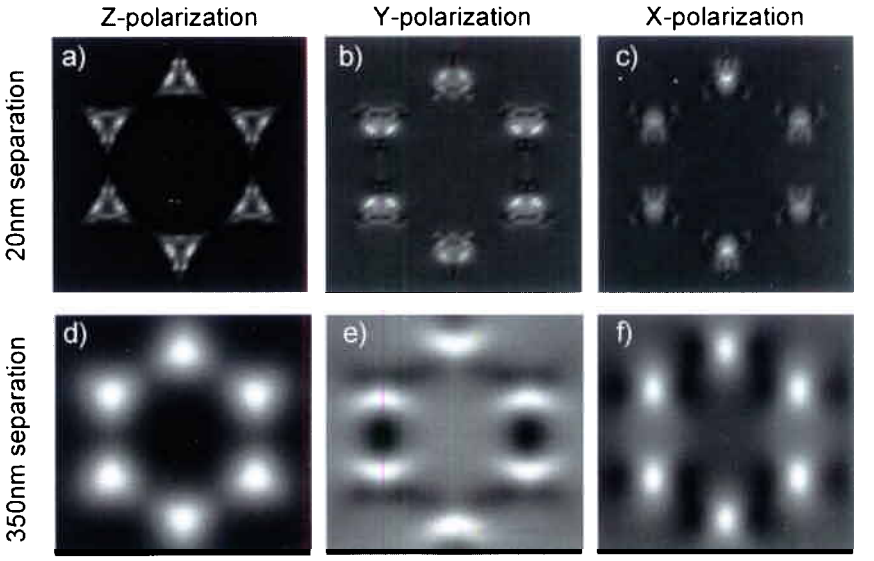

Fig. 38. Simulations considering the transmission of radiation from a dipole with different polarizations at two different separations from the sample.

sub-monolayer of the donor molecules. The illumination of the tip takes place at wavelength λ_1 which can be absorbed by the donor molecules. As the substrate is scanned and a donor molecule is brought into the illumination spot, it absorbs and transfers its energy to the acceptor molecules at the tip. Because the interaction range of the Förster transfer is typically R_0 between 2 nm and 8 nm, one expects a signal only from those acceptor molecules at the very end of the tip and therefore a very high lateral resolution. These experiments are not yet at the single-molecule level, however. In fact, although in principle feasible, due to barriers such as photobleaching order-of-magnitude estimates for such an arrangement are not very favorable at room temperature.

8. – Scanning probe techniques and nano-optics

In this section we go beyond microscopy and discuss some ideas for the wider use of scanning probe techniques and local optical measurements. As we will see, among others an important goal is to combine high-resolution optical spectroscopy with nanometer accuracy in positioning in order to study optical properties of matter at the nanoscale.

8·1. *Combination of force microscopy with confocal microscopy.* In many cases a high optical resolution is not really required. An example of this was shown in fig. 35 where individual molecules were so distanced from each other that they could be easily resolved in a confocal microscope. Nevertheless many researchers use SNOM because, aside from a better optical resolution, it offers information about the sample topography via the shear-force signal. This extra information is particularly of interest in biology where

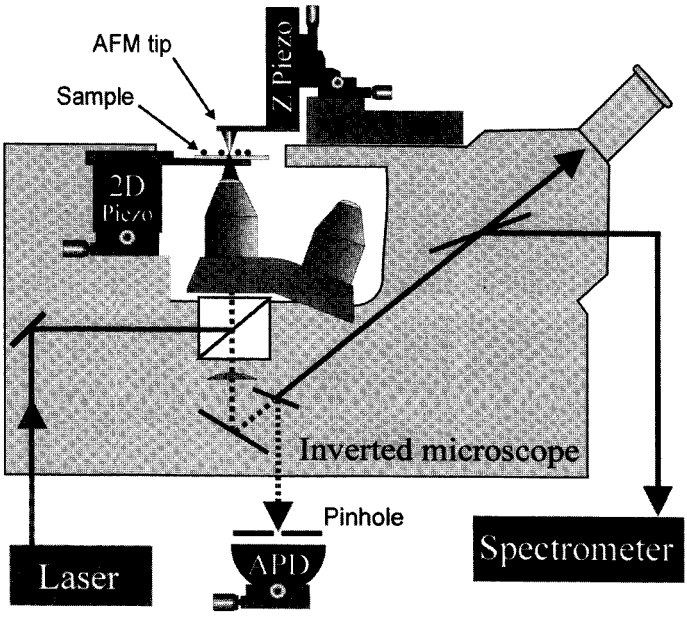

Fig. 39. – Schematic view of a combined AFM-confocal microscope.

samples are not flat and where the topography reveals a great deal about the sample. For several reasons it is often a better idea, though, to use a combined AFM and confocal microscope. First, one has access to higher intensities in a confocal microscope. Second, typically the topography resolution in AFM is up to ten times better than that in SNOM. Third, one has the option of performing optical measurements in the absence of a tip which might perturb the nano-environment of the experiment.

Figure 39 shows a schematic view of the setup in which an AFM is built on an inverted optical microscope with an integrated piezo-scanner that positions the sample. By aligning the AFM tip and the axis of the microscope objective, one can record topography and optical images from the same location of the sample. An example of this is displayed in fig. 40 where dye-doped polymer colloids of 100 nm diameter that have been spin-coated on a glass substrate are imaged [139]. Having seen the AFM image in fig. 40a), the experimentalist can in this particular case identify a single colloid on which optical measurements are to be performed. Let us point out that in some circumstances the presence of the AFM tip might disturb optical measurements. In such cases AFM and confocal scans have to be done sequentially. On the other hand, an AFM tip itself can also be used as a manipulation tool, for example for unfolding proteins [140] and for measuring tiny forces. A combined AFM/confocal microscope provides optical access to such experiments.

8·2. *Characterization of optical micro-systems.* – Combination of scanning probe techniques with optical spectroscopy also holds a great promise for characterization of optical

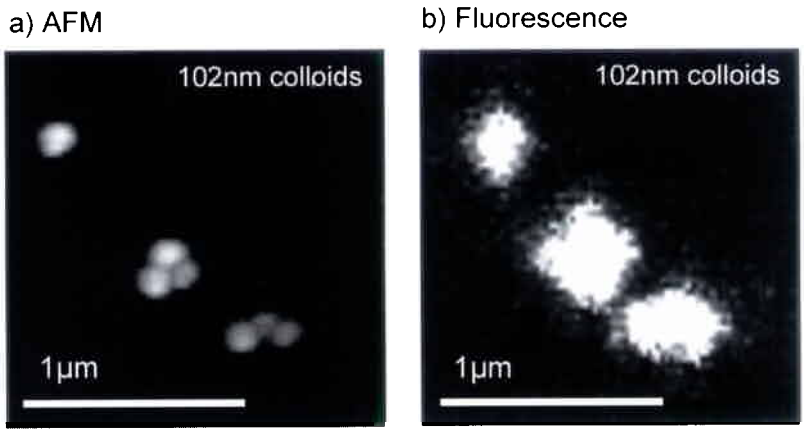

Fig. 40. a) AFM image of dye-doped colloidal particles on a cover glass. b) A fluorescence confocal image of the same area as in a).

systems with nanometer precision. The first example of this was demonstrated in 1994 where a standing evanescent wave on a prism was mapped in PSTM arrangement [53]. This idea has been extended to waveguides [141] and microcavities such as silica microspheres in which very high-Q whispering gallery modes can be excited [54]. Figure 41 depicts an experiment in which an uncoated fiber tip was scanned on contact with a silica microsphere in order to identify the different transverse whispering gallery modes. The importance of this knowledge becomes clear in the next section where we discuss controlled coupling of a nanoparticle to these modes.

Another class of an optical systems that are of current interest are photonic crystals [142]. These are dielectrics that possess periodic modulations of the index of refraction on the length scale of $\lambda/2$, where λ is the wavelength of light. Quite similar to a periodic potential that could give rise to a band gap in the electronic energy of a crystalline structure, a periodic index of refraction in a Maxwell's equation leads to a band gap in the energy of photons traversing through. This is not different from the principle of a Bragg mirror where multiple reflections interfere to substantially lower the transmission of a substrate. The exciting aspect of photonic crystals is their potential for controlling light propagation in all directions and for all polarizations. Moreover, photonic crystals that contain defects allow for localization of light in very confined spaces. Figure 42 displays the top view of two-dimensional crystals made of arrays of air holes in silicon, containing a point defect and a line defect. In the first case one hole is missing, and as a result light can be confined to this region since it cannot propagate in any other direction. This gives rise to a resonance in frequency space and a strong localization of photons to within a fraction of the wavelength, facilitating the control of spontaneous emission for an emitter at that location. The linear defect in fig. 42b) acts as a waveguide that is extremely robust. Calculations have predicted that such a waveguide would stay efficient even if it contained a very sharp bend.

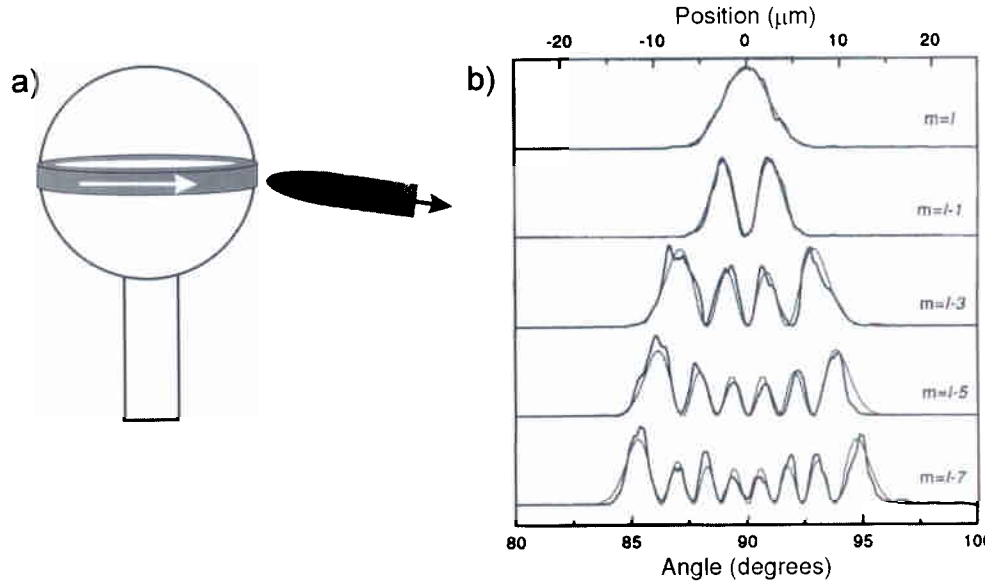

Fig. 41. - a) The schematics of using PSTM for mapping the angular distribution of the intensity circulating in a microsphere. b) Transverse intensity distribution in the evanescent field for different transversal modes. The top curve shows the most desired fundamental mode with the smallest volume. b) is taken from [54].

The very nature of subwavelength index modulations in a photonic crystal suggests the use of near-field methods [143]. In particular, it would be very exciting to have a direct access to the intensity distribution inside such strongly confined geometries. Figure 43 shows a recent measurement in which the function of a photonic crystal beam splitter was put into experimental evidence by local detection of the transmitted light [144]. One clearly resolves the two channels but also sees that light is not distributed uniformly within the waveguide. As is shown in a cross-section, the width of the intensity distribution is considerably less than a wavelength. In the next step the evanescent fields on the upper surface could be probed in a similar way in order to monitor propagation of light in the waveguides and at the splitting junction between them.

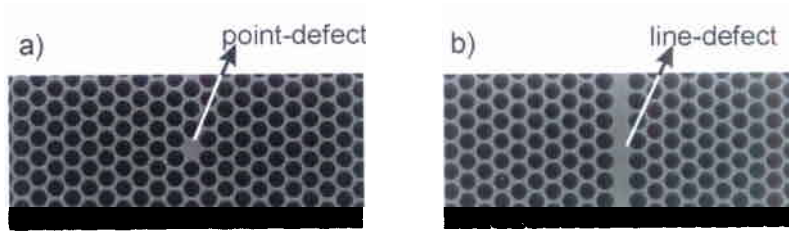

Fig. 42. - The top view of two-dimensional photonic crystals containing defects. The distance between neighboring holes is about 1.5 μm while the wavelength of interest is about 3.5–4 μm.

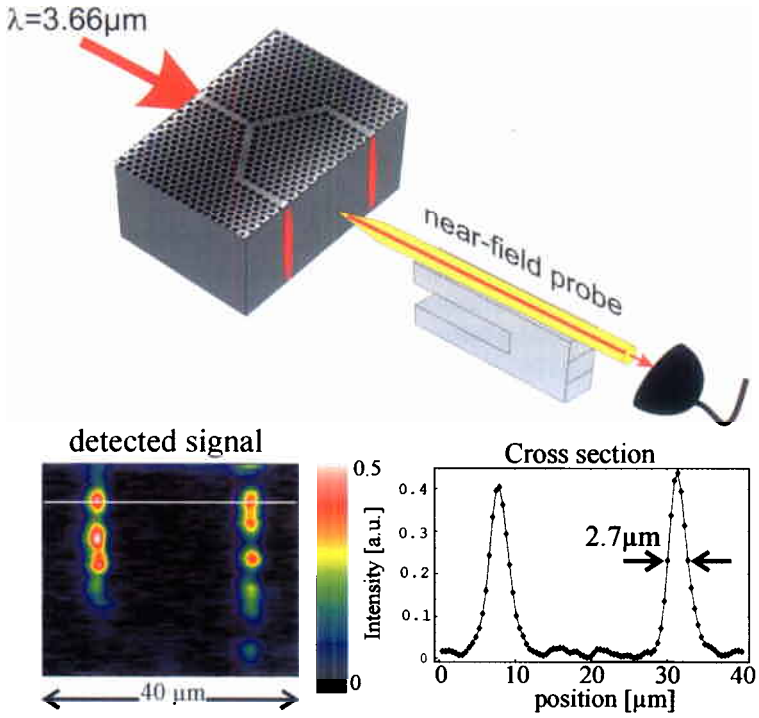

Fig. 43. – An uncoated fiber tip is used to extract light out of the two exit waveguides of a photonic crystal beam splitter. The lower left image shows a two-dimensional map of the intensity at the output plane. A cross-section from this image is displayed in the lower right figure.

8·3. *Photophysics at the nanometer scale.* – In previous sections we have seen that single molecules as well as single gold nanoparticles can be mechanically manipulated with nanometer accuracy. An exciting direction of future research is to place these in confined geometries and to study modifications of their optical properties such as spontaneous emission rate, energy level shifts, energy transfer, or enhancement of weak processes such as Raman transitions. Figure 44 displays some examples. Figure 44a) indicates the possibility of precisely manipulating a molecule in the very immediate vicinity of other molecules that could absorb at the wavelength of the emission from the probe molecule. For very small distances below 10 nm one would be able to study Förster energy transfer. But even at larger separations concepts such as absorption cross-section could be put in question and examined by carefully positioning one dipole moment at subwavelength distances from another dipole.

In figs. 44b) and c) it is suggested that a single molecule and a single metallic particle could be brought very close to each other. We had discussed in a previous section that the electric field near a metallic particle can become considerably large, and we have also seen that this field enhancement could be used for SERS studies. A single molecule and a single gold particle constitute a very well-characterized and reproducibly fabricated system that could offer quantitative information about the role of field enhancements in SERS.

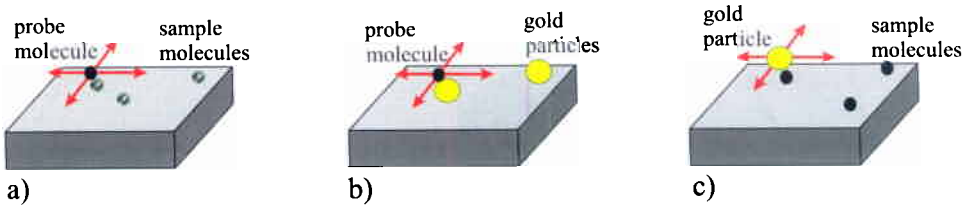

Fig. 44. – Some examples of studying local interactions between nanoparticles and molecules. a) A single molecule (probe) is positioned against other molecules (sample) for a controlled study of their optical interactions such as energy transfer. b) A single molecule is scanned in the near field of a well-defined gold nanoparticle to study field enhancement effects on processes such as SERS. c) Same as in b) but this time the gold particle acts as the probe.

8·4. *Quantum nano-optics.* – In this last section let us briefly examine the possibility of applying scanning probe techniques or using single nanoparticles in quantum optics. Historically all activities in quantum optics and atomic physics have focused on spectroscopy of large ensembles of atoms. Over the years many clever techniques were developed to eliminate inhomogeneities and broadening effects in order to perform precision measurements. With the advent of laser cooling and trapping researchers have realized smaller and better controlled ensembles and indeed even handling of single atoms and ions has been demonstrated [145]. Very recent experiments have shown that one can trap a single atom by a single photon in a high-finesse cavity [146]. However, nearly all these experiments lack a precise knowledge of the position for the atom or ion in question. This is an especially important issue in a high-finesse cavity where the light intensity varies by many orders of magnitude over a fraction of a wavelength. As suggested in fig. 45, it should be possible to approach this problem using nanoscopic solid-state systems such as single molecules or single semiconductor quantum dots. At a first glance it might seem that

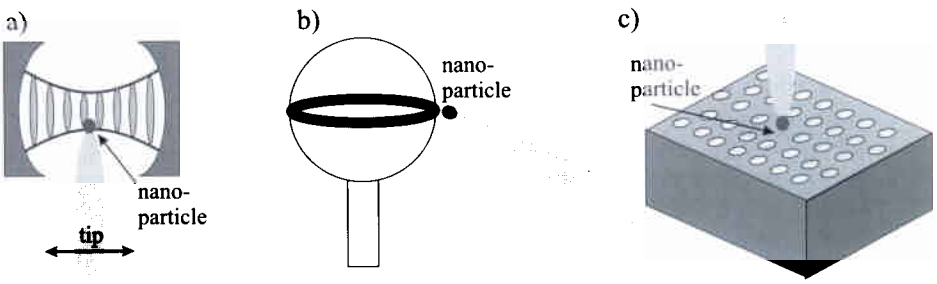

Fig. 45. – A variety of possible microcavity designs for coupling a nanoscopic active medium to photons in a very small mode volume: a) a conventional Fabry-Perot cavity, b) a silica microsphere, c) a photonic crystal with a defect. In each case the position of the active medium plays a decisive role in determining the coupling strength and/or mode selection.

introducing a finite-sized object such as a microcrystal at the end of a tip would strongly reduce the cavity quality factor due to scattering losses. However, our preliminary measurements show that at least in the case of a whispering gallery mode the influence of a tip on the quality factor can be minimized to a level that can be tolerated [147].

9. – Conclusions

In closing, we have discussed the physical grounds for optical microscopy in the near field and various mechanisms for obtaining information about the tiny constituents of a sample. We have seen that, although SNOM has not become as established as AFM and STM, there exists a wide range of ideas that probe different ways of reaching its ultimate limit—the unlimited optical resolution. In particular, apertureless methods using active probes such as a single molecule or passive probes such as sharp tips or single metallic particles hold promise for controlled optical experiments at the nanometer scale.

One has to remember that no microscopy method is universal, and that the best choice of the contrast mechanism depends on the details of the sample and processes to be studied. Even within optical microscopy and within SNOM the researcher should carefully choose the type of probe as well as illumination and collection modes that are suitable for each particular case.

From the point of view of experimental challenge and satisfaction of one's intellectual curiosity, there is no end in sight. There remain many years of hard work to reach the level of performing controlled textbook experiments in which all nano-parameters can be fine-tuned at will. Often at the nanometer scale physics, chemistry, material science and biology all come together and become one. To this end, a complete insight into the properties of matter at this scale requires an interdisciplinary collaboration and interest.

Since writing this chapter we have succeeded in using a diamond nanocrystal containing nitrogen-vacancy color centers as a nanoscopic light source [148]. This system turns out to be fully photostable even at room temperature. The resolution that we have obtained in the laboratory reaches 140 nm at the moment and has high promise for reaching 10–20 nm by using nanocrystals of this dimension.

* * *

I am grateful to D. POHL, C. HENKEL, O. MARTIN and R. CARMINATI for many instructive and fruitful discussions. I would like to thank all my current and former colleagues in the nano-optics group in Konstanz for their excellent work as well as lively and stimulated discussions, especially Friday mornings at breakfast. Thanks are also due to M. BECK who prepared some of the figures in this work. Finally, I am indebted to Prof. J. MLYNEK, for his continuous support and encouragement.

REFERENCES

[1] STROSCIO J. and EIGLER D. M., *Science*, **254** (1991) 1319.
[2] GIMZEWSKI J. and JOACHIM C., *Science*, **283** (1999) 1683.

[3] POHL D. W., DENK W. and LANZ M., *Appl. Phys. Lett.*, **44** (1984) 651.
[4] LEWIS A., ISAACSON M., HAROOTUNIAN A. and MURRAY A., *Ultramicroscopy*, **13** (1984) 227.
[5] POHL D. W., in *Advances in Optical and Electron Microscopy*, edited by C. J. R. SHEPPARD and T. MULVEY (Academic Press, London) 1991, pp. 243-312.
[6] HEINZELMANN H. and POHL D. W., *Appl. Phys. A*, **59** (1994) 897.
[7] COURJON D. and BAINIER C., *Rep. Prog. Phys.*, **57** (1994) 989.
[8] GREFFET J.-J. and CARMINATI R., *Prog. Surf. Sci.*, **56** (1997) 133.
[9] PAESLER M. A. and MOYER P. J., *Near-field Optics, Theory, Instrumentation, and Applications* (Wiley-Interscience) 1996.
[10] LORD RAYLEIGH, *Philos. Mag.*, **8** (1879) 261.
[11] BORN M. and WOLF E., *Princples of Optics* (Pergamon Press) 1993.
[12] SCHMIDT TH., SCHÜTZ G. J., BAUMGARTNER W., GRUBER H. J. and SCHINDLER H., *Proc. Natl. Acad. Sci.*, **93** (1996) 2926.
[13] VAN OIJEN A. M., KÖHLER J., SCHMIDT J., MÜLLER M. and BARAKENHOFF G. J., *Chem. Phys. Lett.*, **292** (1998) 183.
[14] HECHT E., *Optics* (Addison-Wesley Publishing Co.) 1987.
[15] BETZIG E., *Opt. Lett.*, **20** (1995) 237.
[16] WEISS S., *Science*, **283** (1996) 1676.
[17] SALEH B. E. A. and TEICH M. C., *Fundamentals of Photonics* (Wiley-Interscience) 1991.
[18] VOLKMANN H., *Appl. Opt.*, **5** (1966) 1720.
[19] GIRARD C. and DEREUX A., *Rep. Prog. Phys.*, **59** (1996) 657.
[20] GUERRA J. M., *Appl. Opt.*, **29** (1990) 3741.
[21] GUERRA J. M., SRINIVASARAO M. and STEIN R. S., *Science*, **262** (1993) 1395.
[22] MANSFIELD S. M. and KINO G. S., *Appl. Phys. Lett.*, **57** (1990) 2615.
[23] GHISLAIN L. P., ELINGS V. B., CROZIER K. B., MANALIS S. R., MINNE S. C., WILDER K., KINO G. S. and QUATE C. F., *Appl. Phys. Lett.*, **74** (1999) 501.
[24] MASSEY G. A., *Appl. Opt.*, **23** (1984) 658.
[25] VIGOUREUX J. M., DEPASSE F. and GIRARD C., *Appl. Opt.*, **31** (1992) 3036.
[26] VIGOUREUX J. M. and COURJON D., *Appl. Opt.*, **31** (1992) 3170.
[27] SYNGE E. H., *Philos. Mag.*, **6** (1928) 356.
[28] ASH E. A. and NICHOLLS G., *Nature*, **237** (1972) 510.
[29] BETHE H. A., *Phys. Rev.*, **66** (1944) 163.
[30] BOUWKAMP C. J., *Phillips Res. Rep.*, **5** (1950) 401.
[31] BETZIG E. and CHICHESTER R. J., *Science*, **262** (1993) 1422.
[32] DECCA R. S., DREW H. D. and EMPSON K. L., *Appl. Phys. Lett.*, **70** (1997) 1932.
[33] OBERMÜLLER C. and KARRAI K., *Appl. Phys. Lett.*, **67** (1995) 3408.
[34] DREWS D., STOPKA M., MAYR K., LACHER M., EHRFELD W., KALKBRENNER T., GRAF M., SANDOGHDAR V. and MLYNEK J., to appear in *Microelect. Eng.*
[35] MONONOBE S., SAIKI T., SUZUKI T., KOSHIHARA S. and OHTSU M., *Opt. Commun.*, **146** (1998) 45.
[36] LIEBERMAN K., HARUSH S., LEWIS A. and KOPELMAN R., *Science*, **247** (1990) 59.
[37] NOVOTNY L., POHL D. W. and HECHT B., *Opt. Lett.*, **20** (1995) 970.
[38] HUSER J., *Opt. Soc. Am. A*, **16** (1999) 141.
[39] BETZIG E., TRAUTMAN J. K., WEINER J. S., HARRIS T. D. and WOLFE R., *Appl. Opt.*, **31** (1992) 4563.
[40] MARTIN O., *J. Microsc.*, **194** (1999) 235.
[41] GIRARD C., DEREUX A., MARTIN O. J. F. and DEVEL M., *Phys. Rev. B*, **52** (1995) 2889.

[42] HECHT B., BIELEFELDT H., INOUYE Y., POHL D. W. and NOVOTNY L., *J. Appl. Phys.*, **81** (1997) 2492.
[43] SANDOGHDAR V., WEGSCHEIDER S., KRAUSCH G. and MLYNEK J., *J. Appl. Phys.*, **81** (1997) 2499.
[44] MARTIN Y., ZENHAUSERN F. and WICKRAMASINGHE K., *Appl. Phys. Lett.*, **68** (1996) 2475.
[45] JORDAN C. E., STRANICK S. J., RICHTER L. J. and CAVANAGH R. R., *J. Appl. Phys.*, **86** (1999) 2785.
[46] LABARDI M., PATANÈ S. and ALLEGRINI M., *Appl. Phys. Lett.*, **77** (2000) 2042.
[47] SASAKI H. and SASAKI Y., *J. Appl. Phys.*, **85** (1999) 2026.
[48] FISCHER U. C. and ZINGSHEIM H. P., *J. Vac. Sci. Technol. B*, **19** (1981) 881.
[49] KOGLIN J., FISCHER U. C. and FUCHS H., *Phys. Rev. B*, **55** (1997) 7977.
[50] KALKBRENNER T., GRAF M., DURKAN C., MLYNEK J. and SANDOGHDAR V., *Appl. Phys. Lett.*, **76** (2000) 1206.
[51] REDDICK R. C., WARMACK R. J. and FERRELL T. L., *Phys. Rev. B*, **39** (1989) 767.
[52] COURJON D., SARAYEDDINE K. and SPAJER M., *Opt. Commun.*, **71** (1989) 23.
[53] COURJON D., BAINIER C. and BAIDA F., *Opt. Commun.*, **110** (1994) 7.
[54] KNIGHT J. C., DUBREUIL N., SANDOGHDAR V., HARE J., LEFEVRE-SEGUIN V., RAIMOND J. M. and HAROCHE S., *Opt. Lett.*, **20** (1995) 1515.
[55] KNIGHT J. C., DUBREUIL N., SANDOGHDAR V., HARE J., LEFEVRE-SEGUIN V., RAIMOND J. M. and HAROCHE S., *Opt. Lett.*, **21** (1996) 698.
[56] BALISTRERI M. L. M. *et al.*, *Opt. Lett.*, **24** (1999) 1829.
[57] BALISTRERI M. L. M., DRIESSEN A., KORTERIK J. P., KUIPERS L. and VAN HULST N. F., *Opt. Lett.*, **25** (2000) 637.
[58] COURJON D., VIGOUREUX J.-M., SPAJER M., SARAYEDDINE K. and LEBLANC S., *Appl. Opt.*, **29** (1990) 3734.
[59] GIRARD C. and SPAJER M., *Appl. Opt.*, **29** (1990) 3726.
[60] ADELMANN C., HETZLER J., SCHIMMEL T., WEGENER M., WEBER H. and V. LÖHNEYSEN H., *Appl. Phys. Lett.*, **74** (1999) 179.
[61] SPAJER M., BERGOSSI O. and GUIGNARD M., *Opt. Commun.*, **106** (1994) 139.
[62] FISCHER U. C. and POHL D. W., *Phys. Rev. Lett.*, **62** (1989) 458.
[63] SPECHT M., PEDARNIG J. D., HECKL W. M. and HÄNSCH T. W., *Phys. Rev. Lett.*, **68** (1992) 476.
[64] INOUYE Y. and KAWATA S., *Opt. Lett.*, **19** (1994) 159.
[65] ZENHAUSERN F., O'BOYLE M. P. and WICKRAMASINGHE H. K., *Appl. Phys. Lett.*, **65** (1994) 1623.
[66] KAWATA S. and INOUYE Y., *Ultramicroscopy*, **57** (1995) 313.
[67] GLEYZES P., BOCCARA A. C. and BACHELOT R., *Ultramicroscopy*, **57** (1995) 318.
[68] ZENHAUSERN F., MARTIN Y. and WICKRAMASINGHE H. K., *Science*, **269** (1995) 1083.
[69] Private communication with M. LABARDI.
[70] GARCIA N. and NIETO-VESPERINAS M., *Appl. Phys. Lett.*, **66** (1995) 3399.
[71] KNOLL B. and KEILMANN F., *Nature*, **399** (1999) 134.
[72] AIGOUY L., LAHRECH A., GRÉSILLON S., CORY H., BOCCARA A. C. and RIVOAL J. C., *Opt. Lett.*, **24** (1999) 187.
[73] KELLER O., BOZHEVOLNYI S. and XIAO M., in *Near Field Optics*, edited by D. W. POHL and D. COURJON (Kluwer Academic Press) 1993, p. 229.
[74] WESSEL J., *J. Opt. Soc. Am. B*, **2** (1985) 1538.
[75] SUGIURA T., KAWATA S. and OKADA T., *J. Microsc.*, **194** (1999) 291.
[76] BOHREN C. F. and HUFFMAN D. R., *Absorption and Scattering of Light by Small Particles*, (John Wiley & Sons) 1983.

[77] JACKSON J. D., *Classical Electrodynamics* (John Wiley & Sons) 1975.
[78] KALKBRENNER T., RAMSTEIN M., MLYNEK J. and SANDOGHDAR V., *J. Microsc.*, **202** (2001) 72.
[79] ZAYATS A. and SANDOGHDAR V., *Opt. Commun.*, **178** (2000) 245.
[80] JERSCH J., DEMMING F., HILDENHAGEN L. J. and DICKMANN K., *Appl. Phys. A.*, **66** (1998) 29.
[81] VAN BLADEL J., *Singular Electromagnetic Fields and Sources* (Institute of Electrical and Electronics Engineers, Piscataway, N.J.) 1991, p. 165.
[82] CORY H., BOCCARA A. C., RIVOAL J. C. and LAHRECH A., *Microwave & Optical Technology Lett.*, **18** (1998) 120.
[83] AIGOUY L., BOCCARA A. C., RIVOAL J. C., PORTO J. A., CARMINATI R., GREFFET J.-J. and MÉGY R., *Appl. Phys. Lett.*, **76** (2000) 397.
[84] NOVOTNY L., BIAN R. X. and XIE X. S., *Phys. Rev. Lett.*, **79** (1997) 645.
[85] KAWATA Y., XU C. and DENK W., *J. Appl. Phys.*, **85** (1999) 1294.
[86] SANCHEZ E. J., NOVOTNY L. and XIE X. S., *Phys. Rev. Lett.*, **82** (1999) 4014.
[87] STÖCKLE R. M., SUH Y. D., DECKERT V. and ZENOBI R., *Chem. Phys. Lett.*, **318** (2000) 131.
[88] HEITLER W., *The Quantum Theory of Radiation*, 3rd edition (Oxford University Press, Oxford) 1954.
[89] HINDS E. A. and SANDOGHDAR V., *Phys. Rev. A*, **43** (1991) 398.
[90] MILONNI P. W., *The Quantum Vacuum* (Academic Press, Inc., San Diego) 1994.
[91] CHANCE R. R., PROCK A. and SILBEY R., in *Advances in Chemical Physics*, edited by I. PRIGOGINE and S. A. RICE, Vol. **37** (Wiley & Sons, New York) 1978.
[92] BARNES W. L., *J. Mod. Opt.*, **45** (1998) 661.
[93] FORD G. W. and WEBER W. H., *Phys. Rep.*, **113** (1984) 195.
[94] LENNARD-JONES J. E., *Trans. Faraday Soc.*, **28** (1932) 333.
[95] DREXHAGE K. H., in *Progress in Optics XII*, edited by E. WOLF (North-Holland, Amsterdam) 1974, pp. 163-232.
[96] SANDOGHDAR V., SUKENIK C. I., HINDS E. A. and HAROCHE S., *Phys. Rev. Lett.*, **68** (1992) 3432.
[97] ORIA M. *et al.*, *Europhys. Lett.*, **14** (1991) 527.
[98] BAMMEL K. *et al.*, *Chem. Phys. Lett.*, **201** (1993) 101.
[99] LUKOSZ W. and KUNZ R. E., *J. Opt. Soc. Am.*, **67** (1977) 1615.
[100] HELLEN E. H. and AXELROD D., *J. Opt. Soc. Am. B*, **4** (1987) 337.
[101] XIE X. S. and DUNN R. C., *Science*, **265** (1994) 361.
[102] AMBROSE W. P., GOODWIN P. M., MARTIN J. C. and KELLER R. A., *Science*, **265** (1994) 364.
[103] BIAN R. X., DUNN R. C., XIE X. S. and LEUNG P. T., *Phys. Rev. Lett.*, **75** (1995) 4772.
[104] GIRARD C., MARTIN O. J. F. and DEREUX A., *Phys. Rev. Lett.*, **75** (1995) 3098.
[105] NOVOTNY L., *Appl. Phys. Lett.*, **69** (1996) 3806.
[106] RAHMANI A., CHAUMET P. C., DE FORNEL F. and GIRARD C., *Phys. Rev. A*, **56** (1997) 3245.
[107] HENKEL C. and SANDOGHDAR V., *Opt. Commun.*, **158** (1998) 250.
[108] PARENT G., VAN LABEKE D. and BARCHIESI D., *J. Opt. Soc. Am. A*, **16** (1999) 896.
[109] AGARWAL G. S., *Phys. Rev. A*, **11** (1975) 230.
[110] WYLIE J. M. and SIPE J. E., *Phys. Rev. A*, **30** (1984) 1185.
[111] HENKEL C. and SANDOGHDAR V., unpublished.
[112] GERSEN H.-J., GARCIA-PARAJO M. F., NOVOTNY L., VEERMAN J.-A., KUIPERS L. and VAN HULST N. F., *Phys. Rev. Lett.*, **85** (2000) 5312.
[113] LEWIS A. and LIEBERMAN K., *Nature*, **354** (1991) 214.

[114] LIEBERMAN K. and LEWIS A., *Ultramicroscopy*, **42-44** (1992) 399.
[115] KUCK N., LIEBERMAN K., LEWIS A. and VECHT A., *Appl. Phys. Lett.*, **61** (1992) 139.
[116] KURIHARA K., WATANABE K. and OHTSU M., *Proc. of OFS-11* (1996) 694.
[117] STÜRMER H., KÖHLER J. and JOVIN T., *Ultramicroscopy*, **71** (1998) 107.
[118] KRAMPER P., JEBENS A., MÜLLER T., MLYNEK J. and SANDOGHDAR V., *J. Microsc.*, **194** (1999) 340.
[119] GÖTTLICH H. and HECKL W. M., *Ultramicroscopy*, **61** (1995) 145.
[120] HERTZ H. M., MAMQVIST L., ROSENGREN L. and LJUNGBERG K., *Ultramicroscopy*, **57** (1995) 309.
[121] MARTIN J., WANNEMACHER R., TEICHERT J., BISCHOFF L. and KÖHLER B., *Appl. Phys. Lett.*, **75** (1999) 3096.
[122] NIRMAL M., DABBOUSI B. O., BAWENDI M. G., MACKLIN J. J., TRAUTMAN J. K., HARRIS T. D. and BRUS L. E., *Nature*, **383** (1996) 802.
[123] KOPELMAN R. and TAN W., *Science*, **262** (1993) 1382.
[124] SEKATSKII S. K. and LETOKHOV V. S., *Appl. Phys. B*, **63** (1996) 525.
[125] SANDOGHDAR V. and MLYNEK J., *J. Opt. A*, **1** (1999) 523.
[126] See for example articles in *Experimental Technique of Physics, Special issue on Single Molecule Detection* (VCF Weinheim Verlag) 1996.
[127] MOERNER W. E. and KADOR L., *Phys. Rev. Lett.*, **62** (1989) 2535.
[128] ORRIT M. and BERNARD J., *Phys. Rev. Lett.*, **65** (1990) 2716.
[129] NIE S., CHIU D. T. and ZARE R. N., *Science*, **266** (1994) 1018.
[130] TRAUTMAN J. K. and MACKLIN J. J., *Chem. Phys.*, **205** (1996) 221.
[131] SOPER S., NUTTER H. L., KELLER R., DAVIS L. M. and SHERA E. B., *Photochem. Photobiol.*, **57** (1993) 972.
[132] MOERNER W. E. and ORRIT M., *Science*, **283** (1999) 1670.
[133] MICHAELIS J., HETTICH C., MLYNEK J. and SANDOGHDAR V., *Nature*, **405** (2000) 325.
[134] MICHAELIS J., HETTICH C., ZAYATS A., EIERMANN B., MLYNEK J. and SANDOGHDAR V., *Opt. Lett.*, **24** (1999) 581.
[135] MARTIN O., HETTICH C., MICHAELIS J. and SANDOGHDAR V., unpublished.
[136] FÖRSTER TH., *Ann. Phys.*, **2** (1948) 55.
[137] FÖRSTER TH., in *Modern Quantum Chemistry*, edited by O. SINANOGLU (Academic, New York) pp. 93-137.
[138] SHUBEITA G. T., SEKATSKII S. K., CHERGUI M., DIETLER G. and LETOKHOV V. S., *Appl. Phys. Lett.*, **74** (1999) 3453.
[139] SCHNIEPP H., LUDWIG H.-M. and SANDOGHDAR V., unpublished.
[140] KELLERMAYER M. S., SMITH S. B., GRANZIER H. L. and BUSTAMANTE C., *Science*, **276** (1997) 1112.
[141] BOURZEIX S. *et al.*, *Appl. Phys. Lett.*, **73** (1998) 1035.
[142] JOANNOPOULOS J. D., MEADE R. D. and WINN J. N., in *Photonic Crystals* (Princeton University Press) 1995.
[143] FAN S., APPELBAUM I. and JOANNOPOULOS J. D., *Appl. Phys. Lett.*, **75** (1999) 3461.
[144] KRAMPER P., BIRNER A., GÖSELE U., MLYNEK J. and SANDOGHDAR V., unpublished.
[145] MONROE C., MEEKHOF D. M., KING B. E., LEIBFRIED D., ITANO W. M. and WINELAND D. J., *Acc. Chem. Res.*, **29** (1996) 585.
[146] PINKSE P. W. H., FISCHER T., MAUNZ P. and REMPE G., *Nature*, **404** (2000) 365.
[147] GÖTZINGER S., BENSON O. and SANDOGHDAR V., *J. Microsc.*, **202** (2001) 117.
[148] KÜHN S., HETTICH, C., SCHMITT C., POIZAT J.-PH and SANDOGHDAR, *Microsc.*, **202** (2001) 2.